

Heavy Meson Semileptonic Form Factors from Lattice Quantum Chromodynamics

Euan McLean

Supervised by Prof. Christine Davies

*Submitted in fulfillment of the requirements for the degree of
Doctor of Philosophy*

April 2019



*The University of Glasgow
College of Science and Engineering*

Declaration of originality

This thesis is my own work, except where explicit attribution to others is made. In particular Chapters ... are based on the following publications:

All results and figures presented in these chapters are my own, except for ...

'Part of being a winner is knowing when enough is enough. Sometimes you have to give up the fight and walk away, and move on to something that's more productive.'

- Donald Trump

Acknowledgments

I claim sole credit for everything in this thesis.

Contents

1	Introduction	1
2	Motivation & Tools from the Continuum	3
2.1	Testing the Standard Model	3
2.2	Flavour-Changing Charged Currents	5
2.2.1	The CKM Matrix	8
2.2.2	Weak Decays	11
2.2.3	$b \rightarrow c$ Transitions and $ V_{cb} $	15
2.2.4	Flavour Anomalies & Lepton Flavour Violation	18
2.3	Strong Interaction Physics	21
2.3.1	Quantum Chromodynamics	22
2.3.2	Chiral Symmetry	23
2.3.3	Hadrons	25
2.4	Heavy Quark Physics	26
2.4.1	HQET	26
2.4.2	NRQCD	31
3	Lattice Quantum Chromodynamics	33
3.1	Lattice Gauge Fields	34
3.1.1	The Gauge Action	37
3.1.2	Symmanzik Improvements of the Gauge Action	38
3.2	Lattice Fermions	41
3.2.1	The Naive Fermion Action & The Doubling Problem	42
3.2.2	Staggered Quarks	43
3.2.3	Highly Improved Staggered Quarks	45
3.3	Heavy Quarks on the Lattice	47
3.3.1	Heavy HISQ	48
3.3.2	Lattice NRQCD	49
4	Lattice Calculations	51
4.1	Correlation Functions from Lattice Simulations	51
4.1.1	The Path Integral and Generation of Gauge Ensembles	52
4.1.2	Dirac Operator Inversion	52

4.1.3	Staggered Correlation Functions	52
4.2	Analysis of Correlation Functions	56
4.2.1	Non-Linear Regression	57
4.2.2	The Golden Window	61
4.3	Renormalization of Currents	62
4.3.1	Non-perturbative Renormalization of HISQ Currents	64
4.3.2	Matching NRQCD currents to \overline{MS}	64
5	<i>b</i>-Physics from Lattice NRQCD	65
5.1	$B_{(s)} \rightarrow D_{(s)} l \nu$ Form Factors	65
5.1.1	Calculation Setup	65
5.1.2	Results	65
5.1.3	The Subleading Current Problem	65
5.2	Nonperturbative Renormalisation	65
5.2.1	Relativistic Normalisation of the $b \rightarrow c$ Axial Current	65
5.2.2	$b \rightarrow c$ Vector Current Matching to Heavy-HISQ	65
6	$B_s \rightarrow D_s^* l \nu$ Axial Form Factor at Zero Recoil from Heavy-HISQ	67
6.1	Calculation Setup	67
6.2	Results	67
6.3	Implications for $B \rightarrow D^* l \nu$ and $ V_{cb} $	67
7	$B_s \rightarrow D_s l \nu$ Form Factor at All Physical q^2 from Heavy-HISQ	69
7.1	Calculation Setup	69
7.2	Results	69
7.3	HQET low energy constants	69

CHAPTER 1

Introduction

As the LHC continuously refuses to supply new resonances, the high energy physics community places their hope in the intensity frontier to finally break the standard model. Subtle differences between experimental measurements and standard model predictions are the new rock and roll. As collider experiments collect more data and measurements become more precise, theorists must keep up the pace and improve our predictions. What else but Lattice QCD could answer the call of providing first-principle calculations of non-perturbative quantities?

This thesis focuses on the study of calculating form factors for semileptonic $b \rightarrow c$ transitions. These transitions occur between hadrons, bound together by QCD. At the confinement scale ($\sim 1\text{GeV}$), perturbation theory breaks down due to asymptotic freedom, and the only sensible option is to compute the path integral directly.

The b quark is difficult to deal with on the lattice, due to it's mass being beyond the momentum cutoff imposed by computationally feasable lattice spacings. I calculate $b \rightarrow c$ form factors using two approaches to dealing with the heavy b , one employing a non-relativistic action for the b (*NRQCD*), and the other relying on heavy quark effective theory to extrapolate upwards to the b mass (*Heavy-HISQ*). The main take-home from this thesis is the following: **NRQCD is on shaky ground, and Heavy-HISQ is an excellent way to live.**

Using NRQCD, I attempted to compute form factors for the $B_{(s)} \rightarrow D_{(s)} l \nu$ decays. The depletion of the signal/noise ratio in correlation functions featuring high spacial momentum means lattice data for this decay was limited to the high q^2 region.

In NRQCD, flavour-changing current operators are made of an infinite series

of terms in powers of the b -quark velocity v , each requiring their own normalisation via perturbative matching to continuum QCD. It was discovered during this work that subleading terms in this series, that were originally thought to be negligible, in fact may be an important contribution. Since the perturbative matching calculations for these terms have not been performed, this caused a somewhat insurmountable obstacle for the NRQCD approach to calculating $b \rightarrow c$ form factors.

The NRQCD approach could in principle be saved by finding non-perturbative normalizations of these large subleading pieces of the current. We investigated a way of achieving this by comparing NRQCD lattice data to pre-existing and more reliable Heavy-HISQ lattice data, with limited success.

To sidestep the problems with NRQCD, We adopted a totally new approach: the Heavy-HISQ approach. With this, we successfully calculated the $B_s \rightarrow D_s^* l \nu$ axial form factor at zero recoil. This demonstrated the power of the heavy-HISQ approach, and layed the groundwork for a study of $B_s \rightarrow D_s^* l \nu$ form factors away from zero recoil and $B \rightarrow D^* l \nu$ form factors. We also calculated $B_s \rightarrow D_s l \nu$ form factors throughout the full physical range of momentum transfer. These studies, when combined with future experimental data of the $B_s \rightarrow D_s l \nu$ and $B_s \rightarrow D_s^* l \nu$ decays, will supply new tests of the standard model, and new channels to determining the CKM parameter $|V_{cb}|$.

All work reported in this thesis was performed using gluon ensembles courtesy of the MILC collaboration, accounting for dynamical up, down, strange and charm HISQ quarks in the sea. We computed correlation functions using a combination of the MILC code, and HPQCD's NRQCD code.

CHAPTER 2

Motivation & Tools from the Continuum

In this chapter we lay out the physics context of this work, and some theoretical machinery that was useful in our studies. This section consists of a definition and philosophical position of the standard model, with emphasis on quantum chromodynamics. Then, we will expand on the details of the specific sector we are interested in - the flavour sector and the CKM matrix. Finally, we will describe some theoretical framework for studying heavy quarks.

2.1 Testing the Standard Model

need to add: intro to discrete Lorentz symmetries

mention how $SU(3)_C \times SU(2)_L \times U(1)_Y$ relates to electromagnetism via EWSB.

probably need to beef out QCD section a little, maybe a little more intro to hadrons?

add HQET form factors $h_{+,-}$ discussion to HQET section

Neilsen-Ninomaya theorem in sec. 3.2.1?

READING LIST: Lenz, Flavour physics lectures. 1812.11211, 1703.08170

'The B-physics program' :<https://www.ncbi.nlm.nih.gov/pmc/articles/PMC4737432/#andp2015002sec-0020title>

The Standard Model of Particle Physics (SM) is, so far, the most successful theory for describing fundamental particles and their interactions. It is an effective Yang-Mills quantum field theory. It is most succinctly defined by listing its symmetries, field content, and the irreducible representations (irreps) of the symmetries that those fields transform under.

The symmetries are the following. The Lorentz group $SO(3,1)$, the group of coordinate transformations that leave the Minkowski metric invariant, which can be decomposed into $SU(2)_L \times SU(2)_R$ (*left-handed* and *right-handed*). We denote an

irrep as (a, b) where a is the σ^z eigenvalue under $SU(2)_l$ transforms, and b is that of $SU(2)_r$. Then there are internal local gauge symmetries:

$$SU(3)_C \times SU(2)_L \times U(1)_Y, \quad (2.1)$$

irreps of which we denote with (x, y, z) , where x, y are the $SU(3)_C$ and $SU(2)_W$ irreps and z is the charge under $U(1)_Y$.

The field content is: gauge bosons for each generator of the above gauge symmetries, each transforming in the adjoint of their corresponding symmetry and in the $(1/2, 1/2)$ irrep of the Lorentz group, denoted B_μ, W_μ, G_μ respectively. There are 6 $SU(2)_L$ doublets in the $(1/2, 0)$ Lorentz irrep;

$$Q_{1,2,3} = \begin{pmatrix} u_L \\ d_L \end{pmatrix}, \begin{pmatrix} c_L \\ s_L \end{pmatrix}, \begin{pmatrix} t_L \\ b_L \end{pmatrix} , \quad (\mathbf{3}, \mathbf{2}, 1/6) \quad (2.2)$$

$$L_{1,2,3} = \begin{pmatrix} \nu_{e,L} \\ e_L \end{pmatrix}, \begin{pmatrix} \nu_{\mu,L} \\ \mu_L \end{pmatrix}, \begin{pmatrix} \nu_{\tau,L} \\ \tau_L \end{pmatrix} , \quad (\mathbf{1}, \mathbf{2}, -1) \quad (2.3)$$

and 9 $SU(2)_W$ singlets in the $(0, 1/2)$ Lorentz irrep;

$$u_{1,2,3}^R = u_R, c_R, t_R , \quad (\bar{\mathbf{3}}, \mathbf{1}, 2/3) \quad (2.4)$$

$$d_{1,2,3}^R = d_R, s_R, b_R , \quad (\bar{\mathbf{3}}, \mathbf{1}, -1/3) \quad (2.5)$$

$$e_{1,2,3}^R = e_R, \mu_R, \tau_R , \quad (\mathbf{1}, \mathbf{1}, -1) \quad (2.6)$$

We have also listed the SM gauge irreps next to each definition. There is also in principle a further set of right-handed $SU(2)_L$ singlets, $\nu_{1,2,3}^R = (\nu_{e,R}, \nu_{\mu,R}, \nu_{\tau,R})$, but these are singlets of the entire SM gauge group so in a phenomenological sense very much 'not there'. There is also a Lorentz scalar $SU(2)_L$ doublet, the Higgs H , with in Gauge irrep $(1, 2, 1/2)$ that obtains a vacuum expectation value and causes a breaking of the above gauge group, described in the next section.

There is at present no confirmed evidence of physics beyond the SM (or *new physics* (NP)), besides the presence of neutrino (ν) masses. However, there are a number of problems with the SM that heavily imply that there must be new physics. Among the most famous sources of concern are:

- **Dark Matter & Dark Energy** - an estimated 96% of the content of the universe is dark matter and dark energy, that does not interact with the SM gauge group (only via gravity), so cannot be explained by the SM.

- **Matter/Antimatter Asymmetry** - the SM requires there to be an equal amount of matter and antimatter in the universe, however, we observe a massive dominance of matter over antimatter.
- **Neutrino Oscillations** - different species of neutrinos oscillate into each other over time, there is no SM mechanism to explain this.
- **The Hierarchy Problem** - the SM is 'finely tuned', the chances of the Higgs choosing its current vacuum expectation value is estimated to be one in $\sim 10^{45}$.

The central goal of particle physics is currently to pin down evidence against the standard model. Only once we have detailed knowledge of how it breaks down will theorists be able to uniquely determine a new theory of fundamental physics.

There are many promising approaches to achieve this. They are traditionally separated into

- **The Energy Frontier** - explore the highest possible energies reachable with accelerators, directly looking for new physics via the production and identification of new states of matter.
- **The Cosmic Frontier** - use the universe as an experimental laboratory and observatory, taking advantage of naturally occurring events to observe indications of new interactions.
- **The Intensity Frontier** - use intense sources of particles from accelerators, reactors, the sun and the atmosphere to make ultra-precise measurements and find subtle deviations from SM predictions.

The work in this thesis contributes to the third approach. There is a rising tide of more and more SM observables being measured and predicted more and more precisely. It is only a matter of time until one of these observables yields a statistically significant deviation from the SM.

2.2 Flavour-Changing Charged Currents

The SM tests relevant to this work are on quark flavour-changing interactions. Here we will detail the parts of the SM relevant to these interactions.

The $SU(2)_L$ gauge symmetry of the SM is mediated by the vector boson $W = W^1\tau_1 + W^2\tau_2 + W^3\tau_3$, where τ_i are the three $SU(2)$ generators acting on the $SU(2)_L$

doublets defined in the last section. It is convenient to redefine the fields $W = W^+(\tau_0 + i\tau_1) + W^-(\tau_0 - i\tau_1) + W^3\tau_3$. W^\pm, W^3 are the stationary states at low energies due to electroweak symmetry breaking.

The part of the SM lagragian that describes the coupling of W^\pm to fermions is given by

$$\mathcal{L}_{\text{FCCC}} = \frac{e}{\sqrt{2} \sin \theta_W} \left(\bar{u}_L^i W^+ d_L^i + \bar{d}_L^i W^- u_L^i + \bar{\nu}_L^i \bar{W}^+ e_L^i + \bar{e}_L^i W^- \nu_L^i \right) \quad (2.7)$$

where e is the electron charge, θ_W is the Weinberg angle, and $\not{V} = \gamma^\mu V_\mu$ where γ^μ are members of the Clifford algebra acting on fermion spin components. To understand the interactions these terms cause we must also consider the mass terms for the fermions:

$$\mathcal{L}_{\text{mass}} = y_{ij}^u \left(\frac{v}{\sqrt{2}} \right) u_L^i u_R^j + y_{ij}^d \left(\frac{v}{\sqrt{2}} \right) d_L^i d_R^j + y_{ij}^e \left(\frac{v}{\sqrt{2}} \right) e_L^i e_R^j. \quad (2.8)$$

These terms come from the coupling of the fermions to the Higgs field, where the Higgs has taken a vacuum expectation value v at low energies. $y_{ij}^{u,d,e}$ are the Yukawa matrices, parameterising the coupling of the fermions to the Higgs, consisting of free parameters. The absence of right-handed neutrinos forbids an analagous term for neutrinos.

Due to these non-diagnoal mass terms, the fundamental fermion fields are not stationary states. To obtain a more useful representation, one rotates the fields to diagonalise these terms

$$\psi_i^L \rightarrow L_{ij}^\psi \psi_j^L, \psi_R^i \rightarrow R_{ij}^\psi \psi_R^j, \quad (2.9)$$

where $\psi = u, d$ or e , and we fix L_{ij}^ψ, R_{ij}^ψ according to

$$y^\psi \left(\frac{v}{\sqrt{2}} \right) = L^\psi M^\psi R^\psi \quad (2.10)$$

where M^ψ is diagonal. This results in diagonal mass terms, but also has an effect on $\mathcal{L}_{\text{FCCC}}$:

$$\mathcal{L}_{\text{FCCC}} = \frac{e}{\sqrt{2} \sin \theta_W} \left(V_{ij} \bar{u}_L^i W^+ d_L^j + V_{ij}^* \bar{d}_L^i W^- u_L^j + \bar{\nu}_L^i \bar{W}^+ e_L^j + \bar{e}_L^i W^- \nu_L^j \right), \quad (2.11)$$

where $V = L^{u\dagger} L^d$ is by construction a unitary matrix ($V^\dagger V = (L^{d\dagger} L^u)(L^{u\dagger} L^d) = L^d L^{d\dagger} = 1$). V is the famous Cabibbo–Kobayashi–Maskawa (CKM) matrix, consisting of parameters that must be fixed by experiment.

There is no non-diagonal flavour structure in the last two terms, because we have redefined the neutrino fields: $\nu_L \rightarrow L^e \nu_L$, absorbing the rotation of the e_L fields. This can be done with impunity due to the lack of neutrino mass terms. While the SM does not include neutrino mass terms, it has in fact been experimentally confirmed that neutrinos have mass. It is however known that these masses are extremely small in comparison to the scales of the SM ($m_\nu \lesssim 0.05\text{eV}$). Any lepton flavour-changing effect this could in principle have would be much smaller than the current sensitivity of any experiment, for example $\mathcal{B}(\mu \rightarrow \tau\gamma) \simeq 10^{-34}$.

Another useful redefinition is to collect the left-handed and right-handed fermion fields into Dirac spinors ψ :

$$\psi = \psi_L + \psi_R, \quad \psi_L = \frac{1}{2} (1 - \gamma^5) \psi, \quad \psi_R = \frac{1}{2} (1 + \gamma^5) \psi \quad (2.12)$$

In terms of Dirac spinors, $\mathcal{L}_{\text{FCCC}}$ can be written as

$$\mathcal{L}_{\text{FCCC}} = \frac{e}{\sqrt{2} \sin \theta_W} \left(V_{ij} J_\mu^{ij} W^{+\mu} + V_{ij}^* J_\mu^{ij\dagger} W^{-\mu} + L_\mu^{ii} W^{+\mu} + L_\mu^{ii\dagger} W^{-\mu} \right), \quad (2.13)$$

$$L_\mu^{ij} = \frac{1}{2} (\bar{\nu}^i \gamma_\mu e^j - \bar{\nu}^j \gamma_\mu e^i), \quad (2.14)$$

$$J_\mu^{ij} = \frac{1}{2} (\bar{u}^i \gamma_\mu d^j - \bar{u}^j \gamma_\mu d^i) \equiv V_\mu^{ij} - A_\mu^{ij}. \quad (2.15)$$

J_μ^{ij} is known as the Flavour-Changing Charged Current (FCCC), elucidating the mysterious naming of the above Lagrangian. It is often broken up into the *vector* and *axial-vector* components, V_μ and A_μ respectively, since these two components can be categorised according to their transformations under the Lorentz group. V_μ is labelled 1^+ , where the 1 represents its total spin, and the + represents its positive parity $P : V_\mu \rightarrow V_\mu$. A_μ is instead labelled 1^- , due to its negative parity $P : A_\mu \rightarrow -A_\mu$.

We can now turn to the physical consequences of $\mathcal{L}_{\text{FCCC}}$. The interactions given in this part of the Lagrangian describe a quark changing flavour while emitting a W^\pm boson. The propensity for flavour i to decay into another flavour j , is governed in part by energy constraints and in part by the associated CKM element V_{ij} . These interactions at the quark level mediate meson decays, namely leptonic and semileptonic decays, described in section 2.2.2.

The deviation of V_{ij} from a unit matrix breaks some of the symmetries of the SM. $\mathcal{L}_{\text{SM}} - \mathcal{L}_{\text{FCCC}}$ has the property that one can independently rephase each of the quark fields, $q_i \rightarrow e^{i\theta_i} q_i$, a global $U(1)$ symmetry for each quark flavour. This implies, via Noether's theorem, that the number of quarks of each flavour, N_i , is

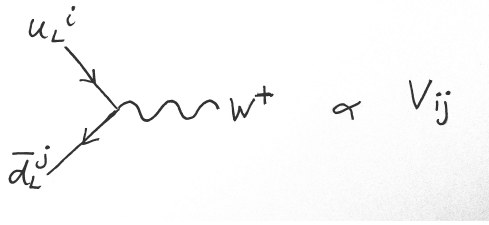


Figure 2.1: The flavour-changing charged current vertex.

conserved. However, $\mathcal{L}_{\text{FCCC}}$ breaks this symmetry $U(1)^6 \rightarrow U(1)$, where there is only a remnant symmetry of transforming all flavours by the same phase. Individual quark flavour number is no longer conserved, but overall quark number is.

Since there is no off-diagonal flavour structure for the Leptons, the equivalent global $U(1)^6$ symmetry for the leptons survives in the SM, and individual lepton flavour number is conserved. This property of the SM is referred to as lepton flavour universality.

2.2.1 The CKM Matrix

The exact values of the CKM matrix elements are of interest in the search for new physics. The CKM matrix is unitary by construction, however, if we were to discover that the values we measure experimentally do not combine to produce a unitary matrix, this would be evidence that the elements we are measuring in fact compose a submatrix of a unitary matrix larger than 3×3 . This would imply the presence of further, heavier quark generations.

Another source of interest in the CKM values is CP violation. CP violation is a global symmetry exhibited by $\mathcal{L}_{\text{SM}} - \mathcal{L}_{\text{FCCC}}$, and physically corresponds to a symmetry between particles and antiparticles. CP violation is one of the famous *Sakarov conditions*, the conditions necessary for a theory to explain the matter/antimatter asymmetry observed in the universe. CP is generically violated when a parameter of the theory has an imaginary component. As will be shown below, the CKM matrix contains one physical phase, making $\mathcal{L}_{\text{FCCC}}$ a source of CP violation. However, the extent of CP violation in the flavour sector is not sufficient to explain the matter/antimatter asymmetry, so the necessary CP violating processes will likely come from new physics beyond the standard model.

To understand the structure of the CKM, we must first ask how many independent physical parameters there are. If one imagines that V is purely real, then it becomes an $SO(3)$ matrix, which can be parameterised by 3 angles, so there are

$N_{\text{real}} = 3$ independent real parameters. A member of $SU(3)$ has 9 independent parameters, so there must be $N_{\text{im}} = N - N_{\text{real}} = 6$ independent phases.

However, we have the freedom to remove some of those phases via a redefinition of the quark fields. $\mathcal{L}_{\text{SM}} - \mathcal{L}_{\text{FCCC}}$ has a global $U(1)^6$ symmetry, a rephasing of each of the 6 quark flavours. One can rephase each flavour without modifying $\mathcal{L}_{\text{SM}} - \mathcal{L}_{\text{FCCC}}$, but with the effect of changing V :

$$V \rightarrow \begin{pmatrix} e^{-ia} & 0 & 0 \\ 0 & e^{-ib} & 0 \\ 0 & 0 & e^{-ic} \end{pmatrix} V \begin{pmatrix} e^{id} & 0 & 0 \\ 0 & e^{ie} & 0 \\ 0 & 0 & e^{if} \end{pmatrix}, \quad (2.16)$$

where $a, b, c, d, e, f \in \mathbb{R}$. So perhaps one can tune each of these 6 phases to remove all 6 phases in V . This is not quite right, we in fact only have the ability to remove 5 of the 6 phases. To see why we can redefine the phases in the following way;

$$V \rightarrow \begin{pmatrix} e^{-ia} & 0 & 0 \\ 0 & e^{-i(a+\alpha)} & 0 \\ 0 & 0 & e^{-i(a+\beta)} \end{pmatrix} V \begin{pmatrix} e^{i(a+\gamma)} & 0 & 0 \\ 0 & e^{i(a+\delta)} & 0 \\ 0 & 0 & e^{i(a+\epsilon)} \end{pmatrix}, \quad (2.17)$$

with $\alpha, \beta, \gamma, \delta, \epsilon \in \mathbb{R}$. a is a useless phase - it will always cancel with itself so cannot be used to remove a phase from V . Hence, one can remove 5 of the 6 phases by redefining the quark fields, leaving one physical phase in the CKM matrix.

This is can be seen as due to the explicit symmetry breaking property of $\mathcal{L}_{\text{FCCC}}$. Inclusion of $\mathcal{L}_{\text{FCCC}}$ breaks the global $U(1)^6$ symmetry down, $U(1)^6 \rightarrow U(1)$, where the broken symmetry is a rephasing of all of the quark flavours by the same amount. This says we can modify $\mathcal{L}_{\text{FCCC}}$ by $N_{\text{broken}} = 5$ independent phases without modifying the rest of the Lagrangian.

So the CKM has 3 real parameters and 1 complex phase. A common parameterisation is

$$V = \begin{pmatrix} 1 & 0 & 0 \\ 0 & \cos \theta_{23} & \sin \theta_{23} \\ 0 & -\sin \theta_{23} & \cos \theta_{23} \end{pmatrix} \begin{pmatrix} 1 & 0 & \sin \theta_{12} e^{i\delta} \\ 0 & 1 & 0 \\ -\sin \theta_{13} e^{i\delta} & 0 & \cos \theta_{13} \end{pmatrix} \begin{pmatrix} \cos \theta_{12} & \sin \theta_{12} & 0 \\ -\sin \theta_{12} & \cos \theta_{12} & 0 \\ 0 & 0 & 1 \end{pmatrix}. \quad (2.18)$$

A useful parameterisation for understanding the relative sizes of the CKM elements is due to Wolfenstein. Define the Wolfenstein parameter $\lambda = \sin \theta_{12}$, which is known experimentally to be around $\lambda \simeq 0.22$. Then $\cos \theta_{12} = \sqrt{1 - \sin^2 \theta_{12}} = \sqrt{1 - \theta^2} \simeq 1 - \lambda^2/2$. Observing then that $\sin \theta_{23} \sim 0.04 \simeq \lambda^2$ and $\sin \theta_{13} \sim 0.004 \simeq \lambda^3/3$, we

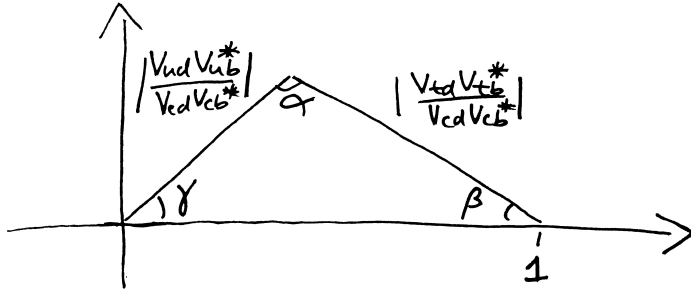


Figure 2.2: A sketch of the unitarity triangle.

can write the matrix as

$$V \simeq \begin{pmatrix} 1 - \frac{1}{2}\lambda^2 & \lambda & \frac{1}{3}\lambda^3 e^{i\delta} \\ -\lambda & 1 - \frac{1}{2}\lambda^2 & \lambda^2 \\ \lambda^3(1 - \frac{1}{3}e^{i\delta}) & -\lambda^2 & 1 \end{pmatrix} = \begin{pmatrix} \mathcal{O}(1) & \mathcal{O}(\lambda) & \mathcal{O}(\lambda^3) \\ \mathcal{O}(\lambda) & \mathcal{O}(1) & \mathcal{O}(\lambda^2) \\ \mathcal{O}(\lambda^3) & \mathcal{O}(\lambda^2) & \mathcal{O}(1) \end{pmatrix} \quad (2.19)$$

There is a clear hierarchy between the values - the CKM matrix is close to the unit matrix. Inter-generational mixing is dominant, dropping from second to first generation is suppressed by λ , dropping from third to second by λ^2 , and dropping from third to first by λ^3 . The SM supplies no compelling explanation of why this hierarchy exists, it is expected that new physics beyond the SM will supply some natural explanation.

The assumption of unitarity in V ,

$$V_{ji}^* V_{jk} = \delta_{ik}, \quad (2.20)$$

imposes 9 constraints on the CKM elements. Each of these constraints gives a test of the SM, if one of these constraints is found to be violated, this represents evidence of new physics. The most studied constraint is given by taking $i = 3, k = 1$;

$$\frac{V_{ud} V_{ub}^*}{V_{cd} V_{cb}^*} + \frac{V_{td} V_{tb}^*}{V_{cd} V_{cb}^*} + 1 = 0. \quad (2.21)$$

This can be visualized as a triangle (known as the *unitarity triangle*) on the complex plane, as shown in figure 2.2.

For unitarity, the triangle must close, in other words, $\alpha + \beta + \gamma = \pi/2$. Hence, to test the CKM unitarity experimentalists measure these angles

$$\alpha = \arg \left(-\frac{V_{td} V_{tb}^*}{V_{ud} V_{ub}^*} \right), \beta = \arg \left(-\frac{V_{cd} V_{cb}^*}{V_{td} V_{tb}^*} \right), \gamma = \arg \left(-\frac{V_{ud} V_{ub}^*}{V_{cd} V_{cb}^*} \right). \quad (2.22)$$

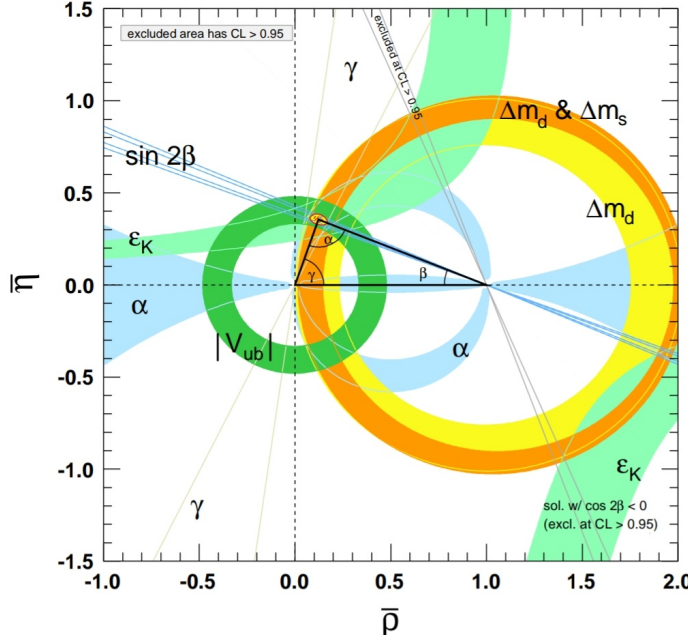


Figure 2.3: Exclusion regions for the vertices of the CKM triangle from various measurements, courtesy of the most recent PDG update [1]

The unitarity triangle also contains information about CP-violation from flavour-changing charged currents. The so-called Jarlskog invariant, $J = \sin \theta_{12} \sin \theta_{23} \sin \theta_{31} \cos \theta_{12} \cos \theta_{23} \cos \theta_{31}^2 \sin \delta$, a measure of CP-violation, is proportional to the area enclosed by the triangle.

The most recent PDG update [1] reports the following averages for the measurements of CKM elements;

$$|V| = \begin{pmatrix} 0.97446 \pm 0.00010 & 0.22452 \pm 0.00044 & 0.00365 \pm 0.00012 \\ 0.22438 \pm 0.00044 & 0.97359^{+0.00010}_{-0.00011} & 0.04214 \pm 0.00076 \\ 0.00896^{+0.00024}_{-0.00023} & 0.04133 \pm 0.00074 & 0.999105 \pm 0.000032 \end{pmatrix}. \quad (2.23)$$

The averages given here are consistent with unitarity in all available tests. For example, taking (2.20) with $i = k = 1$, we find $|V_{ud}|^2 + |V_{us}|^2 + |V_{ub}|^2 = 0.9994 \pm 0.0005$. The angles of the unitarity triangle currently satisfy $\alpha + \beta + \gamma = (180 \pm 7)^\circ$.

Increasing the precision of CKM determinations are necessary to provide more stringent tests of CKM unitarity.

2.2.2 Weak Decays

We now move on to the methods of determining CKM elements. At the confinement scale ($\sim 1\text{GeV}$ and below), quarks are confined by QCD in hadrons. At these energies,

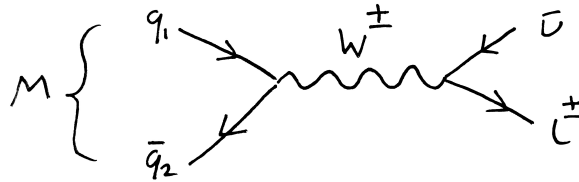


Figure 2.4: Leptonic decay of meson M at tree level in the electroweak coupling.

the dynamics of quarks are only experimentally accessible by probing the dynamics of hadrons. CKM matrix elements are determined by studying hadron decays.

First a word on hadrons. Hadrons are broadly categorized into mesons (charged with one valence quark and one valence antiquark) and baryons (three valence quarks). The entirety of this thesis is concerned with mesons. Mesons are categorized in terms of the flavours they are charged under and their representations under the Lorentz group. We use the notation L^\pm , where L is the meson's spin and \pm denotes its parity. In this thesis we are concerned mostly with pseudoscalar (0^-) and vector (1^-) mesons. A deeper discussion on this is postponed until sec. 2.3.

Weak decays of mesons are categorized according to the final products:

- **Leptonic:** $meson \rightarrow leptons$.
- **Semileptonic:** $meson \rightarrow meson + leptons$.
- **Hadronic:** $meson \rightarrow mesons$.
- **Oscillation:** $meson \rightarrow meson$.

All of these types of decay are dependent on CKM elements so can in principle to be used for studying them. We are most interested in the first two, leptonic and semileptonic, so will give detail of such decays here.

Fig. 2.4 shows a generic leptonic decay at tree level (in electroweak coupling, virtual quark and gluon lines are implicit). The corresponding amplitude is given by

$$\mathcal{M} = \left(\frac{ie}{\sqrt{2} \sin \theta_W} \right) V_{q_1 q_2} \langle l \bar{\nu} | L_\mu^l D_W^{\mu\nu} J_\nu^{q_1 q_2} | M \rangle, \quad (2.24)$$

where D_W is the W^- propagator, $|M\rangle$ is the ground state of the meson M , and $|l \bar{\nu}\rangle$ is a lepton-antineutrino state. We are using the notation $L_\mu^l = L_\mu^{kk}$, where l represents the k th charged lepton. If the momentum of the meson, p^2 , is much

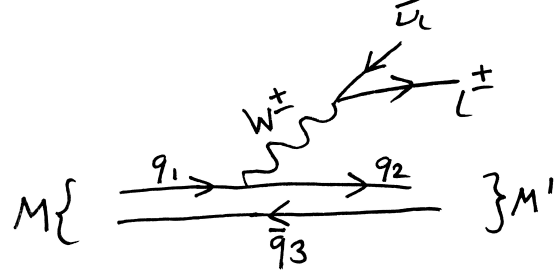


Figure 2.5: Semileptonic decay, $M \rightarrow M' l \bar{\nu}$, at tree level in electroweak coupling.

smaller than the W mass squared, one can integrate out the dynamics of the W to move into the Fermi effective theory [2]:

$$\begin{aligned} \left(\frac{ie}{\sqrt{2} \sin \theta_W} \right)^2 D_W^{\mu\nu}(p^2) &= \left(\frac{ie}{\sqrt{2} \sin \theta_W} \right)^2 \left(\frac{-ig^{\mu\nu}}{p^2 - M_W^2} \right) \\ &= \underbrace{\frac{i}{M_W^2} \left(\frac{ie}{\sqrt{2} \sin \theta_W} \right)^2 g^{\mu\nu}}_{\equiv -2\sqrt{2}G_F} + \mathcal{O}\left(\frac{p^2}{M_W^4}\right). \end{aligned} \quad (2.25)$$

Then \mathcal{M} can be factorised;

$$\mathcal{M} \simeq -2\sqrt{2}V_{q_1 q_2} \langle l \bar{\nu} | L_\mu^l | \Omega \rangle \langle \Omega | J_{q_1 q_2}^{q_1 q_2 \mu} | M \rangle. \quad (2.26)$$

$\langle \Omega | J_{q_1 q_2}^{q_1 q_2} | M \rangle$ is a non-perturbative quantity, since it concerns the transitions of a strongly coupled bound state (QCD at the confinement scale). We know that it has a lorentz index μ , and the only Lorentz vector in the system is the meson's 4-momentum p_μ . So we define

$$\langle \Omega | J_{q_1 q_2}^\mu | M \rangle = p^\mu f_M, \quad (2.27)$$

where f_M is a Lorentz invariant known as the *decay constant* of the meson M , and encodes all non-perturbative information in the amplitude.

By taking the modulus squared of \mathcal{M} , and integrating over all allowed momenta of the final state, one finds the decay rate of the process:

$$\Gamma(M \rightarrow l \bar{\nu}) = \frac{G_F^2}{8\pi} f_M^2 m_l^2 M_M \left(1 - \frac{m_l}{M_M^2} \right)^2 |V_{q_1 q_2}|^2, \quad (2.28)$$

In order to find $|V_{q_1 q_2}|$, one requires both a measurement of $\Gamma(M \rightarrow l \bar{\nu})$, and a value for f_M . f_M can be computed in a Lattice QCD calculation.

A similar story accompanies semileptonic decays. At tree level in the electroweak coupling, a typical semileptonic decay is depicted in fig. 2.8. The amplitude is given

by

$$\begin{aligned}\mathcal{M} &= \left(\frac{ie}{\sqrt{2} \sin \theta_W} \right) V_{q_1 q_2} \langle M', l \bar{\nu} | J_\mu^{q_1 q_2} D_W^{\mu\nu} L_\nu^l | M \rangle \\ &\simeq -2\sqrt{2} G_F V_{q_1 q_2} \langle M', l \bar{\nu} | J_\mu^{q_1 q_2} L^l{}^\mu | M \rangle \\ &\simeq -2\sqrt{2} G_F V_{q_1 q_2} \langle l \bar{\nu} | L^l{}^\mu | \Omega \rangle \langle M' | J_\mu^{q_1 q_2} | M \rangle\end{aligned}\quad (2.29)$$

where on the second line we have integrated out the W propagator in using the same expansion as in the leptonic case, and on the third line we have factorised the QCD part from the electroweak part. The matrix element $\langle M' | J_\mu^{q_1 q_2} | M \rangle$ is a non-perturbative quantity. Unlike in the previous case, there are a number of ways one can choose to parameterise this matrix element, and appropriate choices vary depending on the quantum numbers of M and M' . Of interest to us are the cases where M is a pseudoscalar meson 0^- , and M' is either pseudoscalar or vector 1^- .

In the **pseudoscalar**→**pseudoscalar** case, only the vector component of the current survives in the matrix element, $\langle M' | J_\mu^{q_1 q_2} | M \rangle = \langle M' | V_\mu^{q_1 q_2} | M \rangle$, $\langle M' | A_\mu^{q_1 q_2} | M \rangle$ vanishes since this does not respect the parity invariance of QCD. The most popular parameterisation of $\langle M' | J_\mu^{q_1 q_2} | M \rangle$ is

$$\langle M' | V_\mu^{q_1 q_2} | M \rangle = f_+(q^2) \left[P_\mu + p_\mu - \frac{M^2 - m^2}{q^2} q_\mu \right] + f_0(q^2) \frac{M^2 - m^2}{q^2} q_\mu \quad (2.30)$$

$f_0(q^2)$ and $f_+(q^2)$, known as the scalar and vector form factors, encode all non-perturbative information. We now have non-perturbative functions of q^2 rather than a single number. q^2 , the momentum carried away from the meson by the W , has an allowed range of values if the final states are on-shell;

$$m_l^2 \leq q^2 \leq (M - m)^2. \quad (2.31)$$

By integrating $|\mathcal{M}|^2$ over all final lepton and neutrino momenta, one finds a differential decay rate.

$$\begin{aligned}\frac{d\Gamma}{dq^2}(M \rightarrow M' l \bar{\nu}) &= \eta_{\text{EW}} \frac{G_F^2 |V_{q_1 q_2}|^2}{24\pi^3 M^2} \left(1 - \frac{m_l^2}{q^2} \right)^2 |\mathbf{p}| \times \\ &\quad \left[\left(1 + \frac{m_l^2}{2q^2} \right) M^2 |\mathbf{p}|^2 f_+^2(q^2) + \frac{3m_l^2}{8q^2} (M^2 - m^2)^2 f_0^2(q^2) \right].\end{aligned}\quad (2.32)$$

η_{EW} is the electroweak correction, due to diagrams involving an exchange of a photon or a Z -boson alongside the W between the meson and leptons. \mathbf{p} is the final meson state (M') spacial momentum. Once again, to deduce $|V_{q_1 q_2}|$, one requires both the

decay rates $d\Gamma/dq^2$, and the form factors $f_0(q^2), f_+(q^2)$. To precisely determine the form factors requires a Lattice QCD calculation.

In the **pseudoscalar**→**vector** case, both the vector and axial-vector components of the current survive in the matrix element. A common choice of parameterisation is A common choice of parameterization is

$$\langle M'(\epsilon) | V_{q_1 q_2}^\mu | M \rangle = i\sqrt{Mm} h_V^s(w) \epsilon_{\mu\nu\alpha\beta}^{*\nu} v'^\alpha v^\beta, \quad (2.33)$$

$$\begin{aligned} \langle M'(\epsilon) | A_{q_1 q_2}^\mu | M \rangle &= \sqrt{Mm} [h_{A_1}^s(w)(w+1)\epsilon_\mu^* - \\ &\quad h_{A_2}^s(w)\epsilon^* \cdot v v_\mu - h_{A_3}^s(w)\epsilon^* \cdot v v'^\mu]. \end{aligned} \quad (2.34)$$

$v = P/M$ and $v' = p/m$ are the 4-velocities of M and M' respectively. ϵ is the polarization of the vector meson M' . $w = v \cdot v'$ is known as the recoil parameter, this is an alternative to q^2 often used in heavy quark effective theory. $h_V(w), h_{A_0}(q^2), h_{A_1}(q^2)$, and $h_{A_2}(q^2)$ are the form factors accounting for the non-perturbative physics. The decay rate is given by

$$\frac{d\Gamma}{dw}(M \rightarrow M' l \bar{\nu}) = \frac{G_F^2 m^3 |\eta_{EW} V_{q_1 q_2}|^2}{4\pi^3} (M-m)^2 \sqrt{w^2 - 1} \chi(w) |\mathcal{F}(w)|^2, \quad (2.35)$$

where $\mathcal{F}(w)$ is a linear combination of the form factors, and $\chi(w)$ is a known function of w .

At the zero recoil point, where q^2 is maximized at $q_{\max}^2 = (M-m)^2$, (corresponding to $w = 1$), a single form factor contributes

$$\mathcal{F}(1) = h_{A_1}(1). \quad (2.36)$$

However the differential decay rate vanishes at $w = 1$. A common approach to determine $|V_{q_1 q_2}|$, for example used to find $|V_{cb}|$ via the $B \rightarrow D^* l \bar{\nu}$ decay, is to find $|\mathcal{F}(1)V_{cb}|^2$ at zero recoil by extrapolating from experimental data at non-zero recoil, and combining this with a lattice QCD determination of $h_{A_1}(1)$.

2.2.3 $b \rightarrow c$ Transitions and $|V_{cb}|$

The family of weak decays that have attracted the most attention are decays of B mesons (pseudoscalar mesons containing a valence b and u, d, s or c quark). The B meson decays into a rich variety of decay products. It is the heaviest quark flavour that can be found in hadrons. The only heavier quark, the top quark, has a mass far above the confinement scale, so does not feature as a valence quark in hadrons.

The b can decay into either a charm or an up quark via the flavour changing charged current. In this thesis we are interested in the $b \rightarrow c$ transition, with an

amplitude proportional to the CKM element $|V_{cb}|$. In this section we give a brief overview of how this is calculated and the value's current status.

B meson decays can be measured in a number of experiments. There are two so-called b -factories, the Belle (II) experiment at the KEKB collider in Japan, and the BaBar experiment at the PEP-II collider at SLAC laboratory in the US. These are e^+e^- colliders, that collide with an energy tuned to the mass of the $\Upsilon(4s)$, an excited state of the Υ meson (a 1^- state with $\bar{b}b$ valence quarks). The $\Upsilon(4s)$ has a large branching fraction into a $B\bar{B}$ pair, the decays of these can be measured with large statistics. B decays can also be measured in proton colliders, like the LHCb experiment at CERN. Measurements from LHCb have poorer statistics but cover a larger range of the phase space of final states, due to the variance of momenta in the initial state protons.

So far 3 approaches to determining $|V_{cb}|$ have been carried out.

- $B \rightarrow D^*l\bar{\nu}$ decay rate measurements are extrapolated to zero recoil to determine $|V_{cb}h_{A_1}(1)|$. Then dividing out $h_{A_1}(1)$ from a Lattice calculation, one finds $|V_{cb}|$.
- $B \rightarrow Dl\bar{\nu}$ decay rates are measured throughout q^2 , and combined with $f_0(q^2)$ and $f_+(q^2)$ from lattice calculations.
- $B \rightarrow X_c l\bar{\nu}$ decay rates are measured (where X_c is all possible charmed final state mesons), this is used to constrain elements in the operator product expansion, a method first devised in [3, 4].

The first two are referred to as *exclusive* and the third *inclusive*. A selection of the most accurate examples of each method of determination is given in figure 2.6.

This tells a story of the recent history of $|V_{cb}|$. Determinations from $B \rightarrow Dl\bar{\nu}$ have been consistent but not as precise as via the other two methods. Until recently, there was a 3σ tension between determinations from the $B \rightarrow D^*l\bar{\nu}$ decay, and inclusive decays. This was on its way to being resolved when concern was raised about the method of extrapolating experimental data for $B \rightarrow D^*l\bar{\nu}$ decay rates to the zero recoil point ($w = 1$).

The Heavy Flavour Averaging Group HFAG (Now HFLAV) determination of $|V_{cb}h_{A_1}(1)|$ in 2015 parameterised the form factors in the extrapolation using the CLN parameterisation (defined in section ??). It has become clear that the constraints the CLN parameterisation imposes on the form factors are not justified.

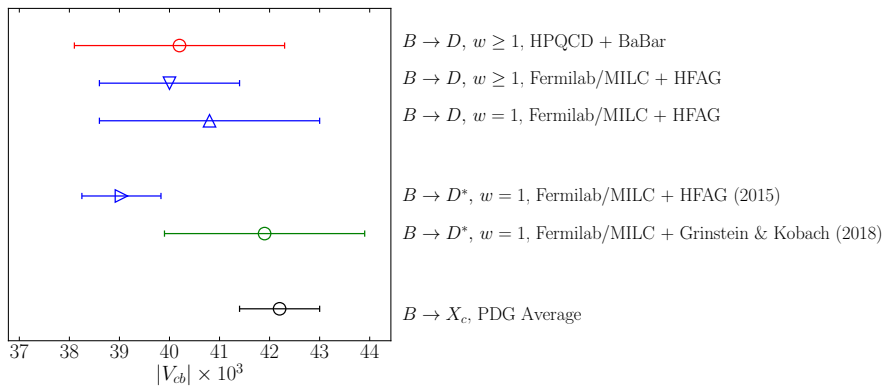


Figure 2.6: Different determinations of $|V_{cb}|$. Points labelled $w = 1$ are determinations from extrapolating measurements of decay rates to the zero recoil point, and combined with a lattice determination of the form factor at zero recoil. Points labelled $w \geq 1$ are results from using a combination of both branching fractions and lattice form factors through some range of w . The first name mentioned in the labels give the source of the lattice form factors, and the second gives the source of the experimental data (e.g. the HPQCD+BaBar point used form factors from the HPQCD collaboration and data from the BaBar experiment. The highest point is from [5], the second and third highest from [6], fourth from [7], fifth from [8]. The bottom point is from the PDG [1], using data from the ALPEPH [9], Belle [10], BaBar [11, 12], and CLEO [13] experiments.

In [8, 14], the results of an extrapolation using the CLN parameterisation were compared to results from a more general, model independent parameterisation, the BGL parameterisation. It was found that they differed by 3.5σ . Since the BGL makes less assumptions, one may consider this the more reliable result.

The $|V_{cb}|$ result using BGL to extrapolate the decay rates is given in the green point on fig. 2.6. Hence, if this work is to be trusted, the long-standing $|V_{cb}|$ tension has been resolved.

There are however a number of other reasons to be interested in studying $|V_{cb}|$, namely improving it's precision. It is currently the least precisely determined element of the CKM matrix. It constrains one side of the unitarity triangle via the ratio $|V_{ub}|/|V_{cb}|$, so it is the bottleneck for precise tests of CKM unitarity. It is also a dominant uncertainty in the determination of the CP -violation parameter ϵ_K (that is currently at tension between the SM and experiment, see for example [15] where a 4σ tension is reported).

A dominant motivation for the work presented in this thesis is the quest for a more precise determination of $|V_{cb}|$. The main results are form factors for $B_s \rightarrow D_s l \bar{\nu}$ and $B_s \rightarrow D_s^* l \bar{\nu}$. The benefit of these determinations are two-fold. Firstly, they can be combined with future experimental measurements of $B_s \rightarrow D_s^{(*)} l \bar{\nu}$ decays for a new $|V_{cb}|$ determination. Increasing the number of independent determinations of $|V_{cb}|$ makes each result more robust. Secondly, they demonstrate that our approach in the lattice calculations work well and can therefore be applied to $B \rightarrow D l \bar{\nu}$ and $B \rightarrow D l \bar{\nu}$ form factors in the future.

2.2.4 Flavour Anomalies & Lepton Flavour Violation

The SM can be tested from studying semileptonic decays more directly, without any consideration of CKM elements. CKM-independent observables can be constructed by taking ratios of branching fractions for decays with common CKM dependence. Then, form factors from lattice QCD can be used to form pure SM predictions of these ratios, and compared to purely experimental measurements of those ratios. Such comparisons have uncovered a number of tensions between the SM and experiment.

The ratios are defined by

$$R_{X_q} = \frac{\Gamma(B_q \rightarrow X_q \tau \nu_\tau)}{\frac{1}{2} [\Gamma(B_q \rightarrow X_q e \nu_e) + \Gamma(B_q \rightarrow X_q \mu \nu_\mu)]} \quad (2.37)$$

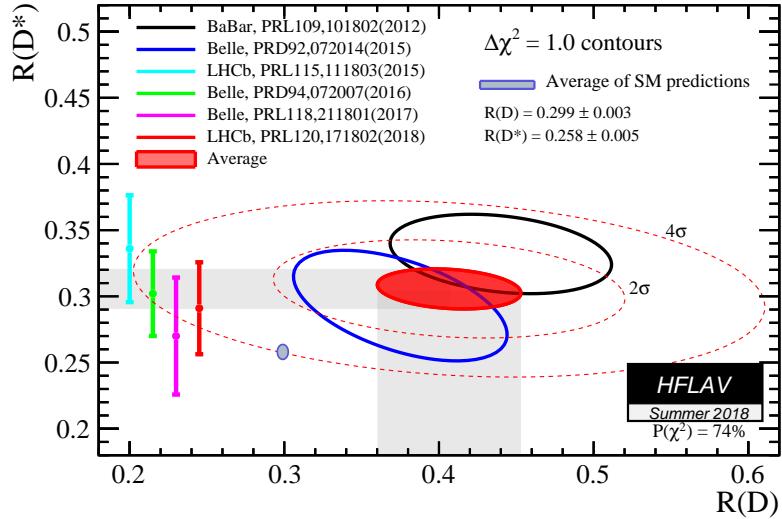


Figure 2.7: $R(D^{(*)})$ determinations from SM and measurement [26]

where X_q is any meson with valence quark content $x\bar{q}$. The numerator and denominator will have the same power of $|V_{bx}|$, so cancel in the ratio.

There is currently tension between SM and experiment in R_D and R_{D^*} .

$$R_{D^*}|_{\text{exp}} = 0.306(13)_{\text{stat}}(07)_{\text{sys}} \quad , \quad R_{D^*}|_{\text{SM}} = 0.252(3) \quad (2.38)$$

$$R_D|_{\text{exp}} = 0.407(39)_{\text{stat}}(24)_{\text{sys}} \quad , \quad R_D|_{\text{SM}} = 0.300(8) \quad (2.39)$$

The experimental values are the HFLAV averages, from BaBar [16,17], Belle [18–21], and LHCb [22–24] data. The $R_{D^*}|_{\text{SM}}$ number is from [25]. The R_D is an average of Lattice results from the HPQCD [5] and FNAL/MILC collaborations [6].

A joint analysis of R_D and R_{D^*} by HFLAV shows the combined tension to have a significance of 4.0σ (see fig. 2.7). Clearly more precise experimental results are necessary to either confirm or dismiss this anomaly. While the SM values are currently much more precise than the experimental ones, further work on the theoretical results are necessary. More independent calculations are required to make the SM numbers more robust, so that, if this tension ever hits 5σ , we can be confident that it is due to new physics.

Besides these, there are also tensions in the quantities [27]:

$$R_{K^{(*)}} = \frac{\Gamma(B \rightarrow K^{(*)}\mu^+\mu^-)}{\Gamma(B \rightarrow K^{(*)}e^+e^-)} \quad (2.40)$$

LHCb measured R_K between 1 and 6 GeV, and found a disagreement with the SM value [?] of 2.6σ [28]. LHCb also measured R_{K^*} in 2 bins ($0.045 < q^2 < 1.1 \text{GeV}^2$ and $1.1 < q^2 < 1.6 \text{GeV}^2$), and reported disagreement with the SM prediction [29–36] of $2.1\text{-}2.3\sigma$ and $2.4\text{-}2.5\sigma$ respectively [37].

A useful direction we could go in, besides improving precision of these ratios, is to test other ratios where LFV should show up. For example, in this thesis we provide a new prediction of R_{D_s} , which when combined with future experimental data, will help elucidate this picture.

Each of these anomalies point to one potential new physics scenario: lepton flavour violation (LFV), a breakdown of the lepton flavour universality in the SM discussed in sec. 2.2. A consequence of LFV would be that the leptons generations would no longer have the same coupling to gauge fields. For example, imagine couplings like $U_{ij}\bar{e}_L^i W^+ \nu_L^j$, where U_{ij} is unitary but non-diagonal, then the different lepton generations would have different couplings to W . This can lead to a modification of the $B \rightarrow D^{(*)}l\nu$ and $B \rightarrow K^{(*)}\bar{l}l$ decays rates by different amounts depending on the lepton flavours in the final state, resulting in the ratios $R_{D^{(*)}}$, $R_{K^{(*)}}$ deviating from the SM prediction.

There are broadly speaking two ways one can explain LFV. The first is to posit that there are in fact right handed neutrinos, ν_R , and neutrinos have Dirac mass terms $m\bar{\nu}_L\nu_R$, from their coupling with the Higgs, just like the charged leptons and quarks. Then, the argument preventing the presence of non-trivial lepton flavour structure in $\mathcal{L}_{\text{FCCC}}$ breaks down, we obtain an equivalent of the CKM matrix for leptons (the Pontecorvo-Maki-Nakagawa-Sakata (PMNS) matrix), and lepton flavour violation is mediated by the W . As already mentioned, neutrinos have been shown to have mass, the PMNS matrix in fact exists, and its elements have been measured. However, as mentioned already, these effects would be extremely small due to the extreme lightness of the neutrinos. Experiments have looked for evidence of W -mediated LFV processes, $\tau \rightarrow \mu\gamma$ and $\mu \rightarrow e\gamma$, and they found upper bounds for their branching fractions of 4.2×10^{-13} [38] and 3.1×10^{-7} [39] respectively.

Besides there being no evidence for W -mediated LFV, this picture of neutrino masses is not very aesthetically satisfying. It requires unnaturally small Yukawa couplings between the Higgs and the neutrinos. The second, and much more popular approach to explaining both LFV and neutrino masses, is the presence of new physics.

In the face of evidence against the SM, the most general way to parameterise

the space of possible new physics models is to study the Standard Model Effective Theory (SMEFT). In this approach, one introduces higher dimension, non-renormalisable operators to the standard model (the SM usually has only renormalisable dimension 4 operators), and impose a hard momentum cutoff Λ . Then, the SMEFT is

$$\mathcal{L}_{\text{SMEFT}} = \mathcal{L}_{\text{SM}} + \sum_i \frac{c_i^{(5)}}{\Lambda} \mathcal{O}_i^{(5)} + \sum_i \frac{c_i^{(6)}}{\Lambda^2} \mathcal{O}_i^{(6)} + \dots \quad (2.41)$$

where $\mathcal{O}_i^{(d)}$ is the set of dimension- d operators that satisfy the SM gauge group, and $c_i^{(d)}$ are coefficients to be measured, known as Wilson coefficients. Any Wilson coefficient measured to be non-zero is evidence that the SM must be augmented with new fields at energies above Λ , and the quantum numbers of the associated operators gives information about the quantum numbers of the new fields.

One can fit the available $B \rightarrow D^{(*)} l \bar{\nu}$ and $B \rightarrow K^{(*)} l \bar{l}$ data to predictions from SMEFT, in order to infer the Wilson coefficients necessary to explain the anomalies.

In [40] it was found that $R_{D^{(*)}}$ can be explained with the operators

$$(\bar{c}\gamma_\mu P_L b)(\bar{\tau}\gamma^\mu P_L \nu_\tau), \quad (\bar{c}\sigma^{\mu\nu} P_L b)(\bar{\tau}\sigma_{\mu\nu} P_L \nu_\tau), \quad (\bar{\tau}P_L c^c)(\bar{b}^c P_L \nu_\tau), \\ (\bar{\tau}\gamma_\mu P_R b)(\bar{c}\gamma^\mu P_L \nu_\tau), \quad (\bar{\tau}\gamma_\mu P_L b)(\bar{c}\gamma^\mu P_L \nu_\tau), \quad (\bar{\tau}P_R c^c)(\bar{b}^c \gamma^\mu P_L \nu) \quad (2.42)$$

where $P_{L/R} = (1 \pm \gamma_5)/2$, $\psi^c = -i(\bar{\psi}\gamma^0\gamma^2)^T$ and $\bar{\psi}^c = -i(\gamma^0\gamma^2\psi)^T$. In [27], a similar process found the operators necessary to explain $R_{K^{(*)}}$:

$$(\bar{s}\gamma_\mu P_L b)(\bar{e}\gamma^\mu e), \quad (\bar{s}\gamma_\mu P_L b)(\bar{\mu}\gamma^\mu \mu) \\ (\bar{s}\gamma_\mu P_L b)(\bar{e}\gamma^\mu \gamma_5 e), \quad (\bar{s}\gamma_\mu P_L b)(\bar{\mu}\gamma^\mu \gamma_5 \mu) \quad (2.43)$$

This information, along with constraints from other measurements, strongly reduces the space of possible new physics models that could produce these anomalies. Hot topics include Leptoquarks, Z' models, and partial compositeness [27, 40–42].

2.3 Strong Interaction Physics

The work of this thesis is essentially quantifying the effect the strong interaction has on branching fractions for semileptonic decays. The strong interaction, and the observed pattern of hadrons, can be explained with a non-abelian Yang-Mills field and a number of flavours of fermions (quarks) that interact with it. In this section we review the fundamental theory, and the force's physical features.

2.3.1 Quantum Chromodynamics

Quantum Chromodynamics (QCD) is an $SU(3)$ Yang-Mills gauge theory. The Lagrangian is derived by requiring:

- N_f fermion fields transforming in the fundamental representation of an $SU(3)$ gauge group.
- Invariance under that gauge group.
- Renormalizability of all interactions.

From these we find [43]

$$\mathcal{L}_{\text{QCD}} = \sum_i \bar{q}_i (iD - m_i) q_i - \frac{1}{4} \text{Tr} G_{\mu\nu} G^{\mu\nu} - g \frac{\theta}{64\pi^2} \epsilon^{\mu\nu\rho\sigma} \text{Tr} G_{\mu\nu} G_{\rho\sigma} \quad (2.44)$$

$$D_\mu = \partial_\mu - igG_\mu, \quad G_{\mu\nu} = [D_\mu, D_\nu]$$

$q_i = (q_{f,r}, q_{f,b}, q_{f,g})$ are the N_f fermions, transforming under

$$q_i(x) \rightarrow \Lambda(x) q_i(x), \quad \bar{q}_f(x) \rightarrow \bar{q}_f(x) \Lambda^\dagger(x), \quad (2.45)$$

where $\Lambda(x)$ is an $SU(3)$ matrix. G_μ are the $\mathfrak{su}(3)$ -valued gluon fields, transforming under the Gauge group like

$$G_\mu(x) \rightarrow \Lambda(x) G_\mu(x) \Lambda^\dagger(x) - \frac{i}{g} [\partial_\mu \Lambda(x)] \Lambda^\dagger(x). \quad (2.46)$$

g is the coupling constant of the theory, often expressed instead as $\alpha_s = (g/4\pi)^2$. $\bar{\theta}$ has strong experimental bounds on its size, to the extent for our purposes it can be neglected [44].

The most notable feature of QCD is due to the running of the QCD coupling α_s [45]. In contrast with the electroweak force, the coupling of the strong force diverges at low energies. This is referred to as *asymptotic freedom*. At energies at and below $\Lambda_{\text{QCD}} \sim 0.3\text{GeV}$, α_s becomes too large to be a good expansion parameter, and perturbation theory becomes unreliable for making predictions.

At large α_s , quarks and gluons become strongly interacting, this is believed to be the source of confinement, the mechanism that binds quarks together into hadrons. A common assumption then is that all of the dynamics that occurs inside hadrons have energies on the scale of Λ_{QCD} .

We arrive at the conclusion that processes involving hadrons cannot be understood using the traditional method of perturbation theory. Broadly speaking there are two alternative approaches:

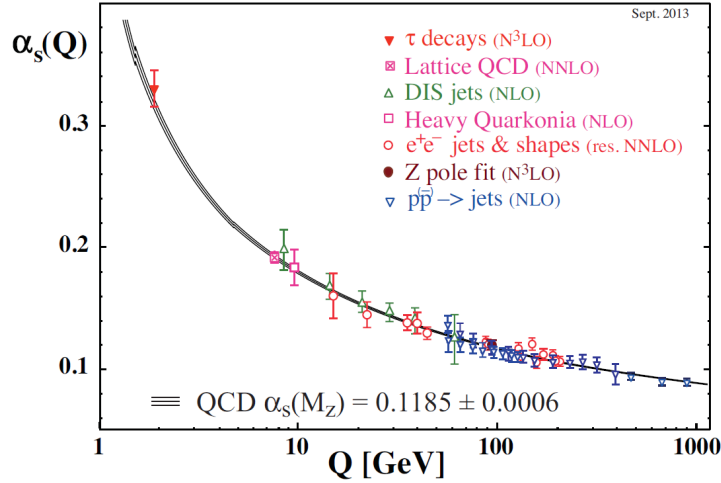


Figure 2.8: The relationship between scale Q and the strong coupling constant α_s , from the PDG [1].

1. Chiral Perturbation theory - an effective theory of hadrons with the same symmetry properties as QCD. This will be introduced in the next section.
2. Lattice simulations - solve the path integral by brute force, eliminating the need for an expansion in α_s . This is covered in chapters 3 and 4, since it is the method used in the work presented in this thesis.

2.3.2 Chiral Symmetry

In the limit of $m_f \rightarrow 0, \forall f$, QCD develops two new global symmetries between the flavours;

$$q_i \rightarrow \exp(i\theta_a \lambda_a^{ij}) q_j \quad (2.47)$$

$$q_i \rightarrow \exp(i\gamma_5 \theta_a \lambda_a^{ij}) q_j \quad (2.48)$$

where λ_a are $U(N_f)$ matrices. They are labelled $U(N_f)_V$ and $U(N_f)_A$ respectively, standing for vector and axial vector. In the below we will take $N_f = 3$ when discussing physical aspects of the symmetry, since in the regime where chiral symmetry is important, the heavier three quarks do not effect the dynamics.

Via Noether's theorem, these symmetries imply currents that are conserved in the massless limit [46];

$$V_\mu^a = \bar{q} \gamma_\mu \lambda_a q \quad , \quad A_\mu^a = \bar{q} \gamma_\mu \gamma_5 \lambda_a q \quad (2.49)$$

The way in which the chiral symmetry is realised in quantum mechanics is captured using the *ward identities*. There are an infinite number of possible ward identities, but for the purpose of our work we only need to consider the most simple of them. We will derive these below.

Consider the partition function for QCD:

$$\mathcal{Z} = \int [d\psi d\bar{\psi} dA] e^{iS[\psi, \bar{\psi}, A]} \quad (2.50)$$

where $[d\psi d\bar{\psi} dA]$ represents the functional integral over quark, antiquark and gauge fields. Consider performing a shift of the integration variables of the form (2.47), and allow the parameters θ_a to be local, $\theta_a = \theta_a(x)$. The partition function becomes

$$\mathcal{Z} = \int \mathcal{J} [d\psi d\bar{\psi} dA] (1 + i\delta S) e^{iS[\psi, \bar{\psi}, A]} \quad (2.51)$$

\mathcal{J} is the Jacobian of the measure $[d\psi d\bar{\psi} dA]$ under the coordinate transform (2.47). In many cases, this will be non-trivial, even if the transform is classically a symmetry of the theory. This can be due to a regularization of the path integral that does not respect the symmetries of the theory, or an anomaly - an instance of a classical symmetry not holding in quantum mechanics. The symmetries we will be concerned with in this work will always be anomaly free, $\mathcal{J} = 1$.

The effect of the local version of (2.47) on the action is

$$\delta S = \int d^4x \theta_a(x) [\partial_\mu V_a^\mu(x) - i\bar{q}(x)[\lambda_a, M]q(x)] \quad (2.52)$$

where $M = \text{diag}(m_u, m_d, m_s, \dots)$ acts on flavour. Setting the arbitrary parameters $\theta_a(x)$ to 1 and removing \mathcal{Z} from each side of (2.51), and removing the spacetime integral $\int d^4x$ results in

$$\partial_\mu \langle V_a^\mu \rangle = i \langle \bar{q}[\lambda_a, M]q \rangle, \quad (2.53)$$

where $\langle \rangle$ represents a quantum expectation value, the state the expectation value is taken need not be specified since the above derivation does not assume any particular state. Repeating the above steps with the vector chiral transform replaced with the axial-vector chiral transform, one finds

$$\partial_\mu \langle A_a^\mu \rangle = i \langle \bar{q}\{\lambda_a, M\}q \rangle \quad (2.54)$$

(2.53) and (2.54) are examples of Ward identities, they describe the non-conservation of the chiral currents.

A useful theorem [47] is that partially conserved currents (currents that become conserved when some parameter in the theory vanishes, like V_{ij}^μ and A_a^μ) require no renormalisation under any regularisation scheme. We will now demonstrate this.

The conserved or partially conserved current J_a^μ has a corresponding charge $Q_a(t) = \int d^3x J^0(\underline{x}, t)$ that is the generator of it's corresponding symmetry transform on Hilbert space. In this case, these charges are members of the Lie algebra of the symmetry group;

$$[Q_a(t), Q_b(t)] = if_{abc}Q_c(t), \quad (2.55)$$

where f_{abc} are the structure constants of the algebra. Under some regularisation, change in regularisation scheme, or running of scale, each operator in the theory may require multiplicative renormalisations; $Q_a \rightarrow Z_Q Q_a$. Equation (2.55) demands that $Z_Q = 1$, So J^0 obtains no renormalisation, and if the regularization is lorentz invariant, this carries on to J^μ .

In the case of the chiral currents V_a^μ, A_a^μ , the Ward identities (2.53), (2.54) cause this property to carry onto the operators on the LHS, $\bar{q}[\lambda_a, M]q$ and $\bar{q}\{\lambda_a, M\}q$, these operators receive no normalisation under any regularisation scheme.

Since one can transform any flavour into any other flavour via the chiral $U(N_f)$ generators, one can build currents charged with any combination of flavours from linear combinations of V_a^μ and A_a^μ ;

$$V_{ij}^\mu = \bar{q}_i \gamma^\mu q_j, \quad \partial_\mu \langle V_{ij}^\mu \rangle = i(m_i - m_j) \langle S_{ij} \rangle \quad (2.56)$$

$$A_{ij}^\mu = \bar{q}_i \gamma^\mu \gamma^5 q_j, \quad \partial_\mu \langle A_{ij}^\mu \rangle = i(m_i + m_j) \langle P_{ij} \rangle \quad (2.57)$$

where we have defined $S_{ij} = \bar{q}_i q_j$ and $P_{ij} = \bar{q}_i \gamma^5 q_j$, the scalar and pseudoscalar densities. The non-renormalisation of V_a^μ and A_a^μ carry on to V_{ij}^μ and A_{ij}^μ , and onto the operators $(m_i - m_j)S_{ij}$, $(m_i + m_j)P_{ij}$ via the Ward identities.

The partially conserved currents V_μ^{ij} and A_μ^{ij} are the same currents that feature in the matrix element of leptonic and semileptonic decays in sec. 2.2, and their expectation values appear in amplitudes for leptonic and semileptonic decays. Hence, the fact that these can be related to alternative expectation values via ward identities, and that they obtain no renormalisation, is very useful in the calculation of these amplitudes. We take advantage of these properties in our lattice calculations.

2.3.3 Hadrons

some categorization of hadrons, just a space to define names, namely of B, B_s, π, K etc.

2.4 Heavy Quark Physics

Quarks with mass $m_Q \gg \Lambda_{\text{QCD}}$ are referred to as heavy quarks. Charm and bottom quarks are considered heavy: $\Lambda_{\text{QCD}}/m_c \sim 1/4$, $\Lambda_{\text{QCD}}/m_b \sim 1/14$. This separation of scales can come in very useful. They mean one can integrate out the degrees of freedom at m_Q , and still have a good description of the dynamics at Λ_{QCD} . As will be demonstrated, this does not mean totally removing the heavy quark from the theory.

The physical picture of a meson containing a heavy quark is very similar to that of a hydrogen atom. In the hydrogen atom, the nucleus has a mass much greater than the characteristic energies of the electron and photons. One can treat the nucleus as a static source of electric charge, and solve to high precision the dynamics of the electron. The electron's behaviour is not affected by the mass or the spin of the nucleus. Similarly, one can consider a heavy quark in a meson to be a static source of color charge, and solve the Λ_{QCD} dynamics in its presence. The mass and spin of the heavy quark does not effect the light degrees of freedom, this is the well understood *heavy quark symmetries*. The effective field theories introduced in this section gives us a framework to take this approximation and systematically correct for it.

2.4.1 HQET

This thesis is concerned with the decays of mesons containing heavy quarks. Heavy Quark Effective Theory (HQET) is an effective field theory with the cutoff at the heavy quark mass m_Q , and terms organized in a series in Λ_{QCD}/m_Q . Since at the b (and c) mass QCD is perturbative ($\alpha_s(m_Q) \ll 1$), one can match HQET to perturbative QCD at m_Q , then run the couplings of HQET down to produce useful predictions at the confinement scale.

It is a useful tool for when we perform extrapolations in heavy quark mass, as it supplies us with explicit expressions for the heavy quark mass dependence on various phenomenological quantities.

HQET Lagrangian

As a simple example, we will derive HQET for a single heavy quark interacting with gluons. The fermion part of the Lagrangian is

$$\mathcal{L}_{\text{QCD}} = \bar{Q}(iD - m_Q)Q, \quad (2.58)$$

where Q is the heavy quark field. Define the heavy quark velocity v according to

$$v = \frac{p_Q}{m_Q}. \quad (2.59)$$

Now split Q into "heavy" and "light" components:

$$Q = h + H \quad : \quad h = \frac{1}{2}e^{-im_Q v \cdot x}(1 + \not{v})Q \quad (2.60)$$

$$H = \frac{1}{2}e^{-im_Q v \cdot x}(1 - \not{v})Q \quad (2.61)$$

with the important property

$$\not{v}h = h \quad \not{v}H = -H. \quad (2.62)$$

In terms of these new fields the Lagrangian becomes

$$\mathcal{L}_{\text{QCD}} = i\bar{h}(v \cdot D)h - \bar{H}(i(v \cdot D) - 2m_Q)H + i\bar{h}\not{D}^\perp h + i\bar{H}\not{D}^\perp h. \quad (2.63)$$

where $v_\mu(v \cdot D)$ is the covariant derivative projected along the direction of v , and $D^\perp = D - v_\mu(v \cdot D)$ are the components perpendicular to v . In the rest frame of the heavy quark, $v = (1, 0, 0, 0)$ so $v_\mu(v \cdot D)$ becomes the temporal derivative and D^\perp the spacial. A physical interpretation of the definition of h in (2.60) can be seen by acting a spacial derivative on the definition of h , and by recognising $\partial Q = -ip_Q$, $\partial h = -ip_h$, we find that

$$p_Q = m_Q v + p_h \quad (2.64)$$

Since $p_h \ll p_Q$, we see that the quark's momentum is dominated by it's mass (the quark is close to on-shell), and the h field represents perturbations around on-shell due to interactions with the lighter degrees of freedom at Λ_{QCD} .

From (2.63), we see that h is a massless field and H has a mass of $2m_Q$. From this Lagrangian we can derive an equation of motion for H :

$$(i(v \cdot D) + 2m_Q)H = i\not{D}^\perp h, \quad (2.65)$$

with the solution

$$H = \frac{1}{i(v \cdot D) + 2m_Q} i\mathcal{D}^\perp h = \frac{1}{2m_Q} \sum_{n=0}^{\infty} \frac{(-i(v \cdot D))^n}{2m_Q} \mathcal{D}^\perp h. \quad (2.66)$$

By substituting this into the Lagrangian we arrive at

$$\mathcal{L}_{\text{HQET}} = i\bar{h}(v \cdot D)h - \bar{h}\mathcal{D}^\perp \frac{1}{2m_Q} \sum_{n=0}^{\infty} \frac{(-i(v \cdot D))^n}{2m_Q} \mathcal{D}^\perp h. \quad (2.67)$$

Since we expect $v \cdot D \sim \Lambda_{\text{QCD}}$, we can interpret the infinite sum as a series in Λ_{QCD}/m_Q , and truncate it at some order. For example to $\mathcal{O}(\Lambda_{\text{QCD}}/m_Q)$, we have

$$\mathcal{L}_{\text{HQET}}^1 = i\bar{h}(v \cdot D)h - \frac{1}{2m_Q} \bar{h}\mathcal{D}^{\perp 2}h \quad (2.68)$$

Leading order HQET exhibits new symmetries not present in full QCD, known as the heavy quark symmetries. Since m_Q is not present in the leading order Lagrangian, there is a flavour symmetry - a set of N heavy quarks with the same v can be mixed via an $SU(N)$ symmetry. Similarly due to the absence of spin mixing matrices, a heavy quark has an $SU(2)$ spin symmetry. This builds up a physical picture of a heavy quark in a meson being a static colour charge, the dynamics at Λ_{QCD} are not effected by it's mass or spin.

Isgur-Wise Function

A consequence of heavy quark symmetry relevant to semileptonic decays are the Wigner-Eckart theorems. Consider a transition amplitude between two heavy pseudoscalar mesons:

$$\langle M(v)|\bar{h}\Gamma h|M(v')\rangle \quad (2.69)$$

The spin structure of $|M(v)\rangle$ is $\gamma_5(1-\not{v})$, this can be shown with the following argument. The state can be generally written as $|M(v)\rangle = \int d^4x d^4y f(x, y)\bar{h}(x)\gamma_5 q(y)|\Omega\rangle$ where q is the light valence quark and $|\Omega\rangle$ is the interacting vacuum. Using $\not{v}h = h$, this can be reexpressed as $|M(v)\rangle = \int d^4x d^4y f(x, y)\bar{h}(x)\gamma_5(1-\not{v})q(y)|\Omega\rangle/2$.

The amplitude can be written as

$$\langle M(v)|\bar{h}\Gamma h|M(v')\rangle = m_M \text{Tr}[\frac{1}{2}\gamma_5(1-\not{v})\Gamma\frac{1}{2}\gamma_5(1-\not{v}')\mathcal{M}(v, v')] \quad (2.70)$$

where $\mathcal{M}(v, v')$ can be any gamma-matrix valued function. The m_M factor comes from the relativistic normalisation of the states. A general spin decomposition of this is

$$\mathcal{M}(v, v') = \xi_0(v \cdot v') + \not{v}\xi_1(v \cdot v') + \not{v}'\xi_2(v \cdot v') + \not{v}\not{v}'\xi_4(v \cdot v'). \quad (2.71)$$

Plugging this into (2.70), we can then write the amplitude in terms of a single function:

$$\langle M(v)|\bar{h}\Gamma h|M(v')\rangle = m_M \text{Tr}[\frac{1}{2}\gamma_5(1-\not{v})\Gamma\frac{1}{2}\gamma_5(1-\not{v}')]\xi(v\cdot v') \quad (2.72)$$

where $\xi(v\cdot v') = \xi_0(v\cdot v') + \xi_1(v\cdot v') - \xi_3(v\cdot v') - \xi_4(v\cdot v')$ is known as the Isgur-Wise function. For a general pair of mesons with spin structure $\mathcal{H}, \mathcal{H}'$, a transition amplitude between them with a heavy current insertion can always be written as

$$\langle \mathcal{H}|\bar{h}\Gamma h|\mathcal{H}'\rangle = \xi(v\cdot v') Tr[\bar{\mathcal{H}}\Gamma\mathcal{H}] + \mathcal{O}\left(\frac{\Lambda_{\text{QCD}}}{m_Q}\right) \quad (2.73)$$

So all heavy semileptonic decays involving any combination of masses or spins are described by a single non-perturbative function, $\xi(v\cdot v')$. Examples relevant to the work of this thesis are:

$$\langle D(v')|c_{v'}^-\gamma^\mu b_v|\bar{B}(v)\rangle = \sqrt{m_B m_D}(v+v')^\mu \xi(v\cdot v') \quad (2.74)$$

$$\langle D^*(v')|c_{v'}^-\gamma^\mu b_v|\bar{B}(v)\rangle = i\sqrt{m_B m_{D^*}}\epsilon^{\mu\nu\alpha\beta}\varepsilon_\nu^* v'_\alpha v_\beta \xi(v\cdot v') \quad (2.75)$$

$$\langle D^*(v')|c_{v'}^-\gamma^\mu\gamma_5 b_v|\bar{B}(v)\rangle = \sqrt{m_B m_{D^*}}[\varepsilon^{*\mu}(v\cdot v' + 1) - v'^\mu \varepsilon^* \cdot v] \xi(v\cdot v'). \quad (2.76)$$

Here we have subscripted the fields $c_{v'}, b_v$ to specify the velocity used to separate those fields from the heavy components e.g. in eq. (2.60).

The Ademollo-Gatto Theorem and Luke's Theorem

Luke's theorem, which can be derived from the Ademollo-Gatto (AG) theorem, tells us the leading order heavy quark mass dependance of form factors. First we will derive the AG theorem. We will follow the proof given in [48].

Consider the transition amplitude

$$\langle \alpha | Q_a | \beta \rangle \quad (2.77)$$

where Q_a is a conserved charge associated with some global symmetry \mathcal{G} , and $|\alpha\rangle$ and $|\beta\rangle$ belong to an irrep of \mathcal{G} . Imagine explicitly breaking the symmetry with a term like $\mathcal{L}_{\text{break}} = \lambda \mathcal{O}_{\text{break}}$. The states in the broken theory can be expressed as

$$|\beta\rangle = c_{\beta\beta}|\beta'\rangle + \sum_m c_{\beta m}|m'\rangle \quad (2.78)$$

$$\langle \alpha | = c_{\alpha\alpha}^* \langle \alpha' | + \sum_n c_{\alpha n}^* \langle n' |. \quad (2.79)$$

where primed states are the new basis of states belonging to irreps of \mathcal{G} , after the breaking. Here $|m'\rangle$ can only be states that can be mixed with $|\beta\rangle$ by $\mathcal{O}_{\text{break}}$, i.e., via the broken dynamics of the theory. Similarly for $\langle n'|$ and $\langle \alpha|$. The transition amplitude becomes

$$\begin{aligned} \langle \alpha | Q_a | \beta \rangle &= c_{\alpha\alpha}^* c_{\beta\beta} \langle \alpha' | Q_a | \beta' \rangle \\ &+ \sum_m c_{\alpha\alpha}^* c_{\beta m} \langle \alpha' | Q_a | m' \rangle \\ &+ \sum_n c_{\alpha n}^* c_{\beta\beta} \langle n' | Q_a | \beta \rangle \\ &+ \sum_m \sum_n c_{\alpha n}^* c_{\beta m} \langle n' | Q_a | m' \rangle \end{aligned} \quad (2.80)$$

The theorem applies to the situation where $|n'\rangle$ and $|m'\rangle$ live in different \mathcal{G} irreps to $|\alpha\rangle$ and $|\beta\rangle$ (we assume $|\alpha\rangle$ and $|\beta\rangle$ to be in the same irrep otherwise the transition amplitude will always be zero). In this case the amplitudes in the second and third terms vanish. Now consider the order of the coefficients c_{nm} . We can assume that $c_{nm} = \mathcal{O}(\lambda)$ for arbitrary $n, m \neq \alpha, \beta$, since switching off the symmetry breaking by setting $\lambda = 0$ should cause $|\alpha\rangle$ and $|\alpha'\rangle$ to coincide. Then, using the normalization of the states $\sum_n |c_{\alpha n}|^2 = 1$, we find $c_{\alpha\alpha} = \sqrt{1 - \mathcal{O}(\lambda)^2} = 1 + \mathcal{O}(\lambda^2)$, and similarly for $c_{\beta\beta}$. Applying this to the two surviving terms in (2.80), we end up with

$$\langle \alpha | Q_a | \beta \rangle = 1 + \mathcal{O}(\lambda^2) \quad (2.81)$$

This is the AG theorem: if the current Q_a and the symmetry breaking therm \mathcal{O} act orthogonally on the states, the transition amplitude can have at most a second order correction in the symmetry breaking parameter.

Now we will apply this to HQET to produce Luke's theorem. Consider a transition including two heavy quarks (b and c). Then, the heavy quark symmetry is a spin symmetry for each flavour, and a flavour symmetry between them. The leading order spin symmetry breaking terms can be found from (2.68) to be

$$\frac{1}{4m_Q} \bar{h} \gamma^\mu \gamma^\nu F_{\mu\nu} h \quad (2.82)$$

for both $h = b$ and $h = c$. The leading order flavour breaking term is

$$\left(\frac{1}{2m_b} - \frac{1}{2m_c} \right) \frac{1}{2} \bar{h} \sigma_z \not{D}^{\perp 2} h \quad (2.83)$$

where now $h = (b, c)$ and the σ_z is the third pauli matrix acting on flavour. These terms cause states, for example $|B\rangle$ to mix with states $|n'\rangle$, each being of the order of

at least one of the following: $1/2m_b, 1/2m_c$, and $(1/2m_b - 1/2m_c)$. It can be shown [48] that the leading order symmetry breaking terms can only mix pseudoscalar and vector mesons with other irreps of the heavy quark symmetries. Hence, for example, in the $B \rightarrow D$ transition we can write

$$\langle D | \bar{c} \gamma_\mu b | B \rangle = 1 + \mathcal{O}((\epsilon_b - \epsilon_c)^2). \quad (2.84)$$

$$\langle D | \bar{c} \gamma_\mu \gamma_5 b | B \rangle = 1 + \mathcal{O}((\epsilon_b - \epsilon_c)^2). \quad (2.85)$$

where we have now defined $\epsilon_h = 1/2m_h$.

2.4.2 NRQCD

An effective field theory closely related to HQET is Non-Relativistic QCD (NRQCD). This differs from HQET only by the power counting; instead of organizing terms in the Lagrangian according to their order in Λ_{QCD}/m , the terms are organized in terms of orders of the heavy quark's spacial velocity $v \sim |\mathbf{p}|/m$. NRQCD is derived with the following process:

- Separate the quark and antiquark components of the heavy quark. Since a non-relativistic fermion is decoupled from its antiparticle, our action only requires to describe the top two components of the spinor. Define the antiquark-free 2-component spinor h via the Foldy-Wouthuysen transformation $\psi \rightarrow \psi_+ = e^{\gamma \cdot \mathbf{D}/2m} \psi$ [49]. This acts to remove the $\gamma \cdot \mathbf{D}$ term from the Dirac part of the Lagrangian, which is the only part that couples the fermion to the anti-fermion.
- Define power-counting by considering the expected expectation values of operators for heavy mesons [50]. The three relevant scales concerning the heavy meson are $M, p \sim Mv$ and $E_K \sim Mv^2$, where M is the meson mass, p the spacial momentum and E_K the kinetic energy. By relating operators to these three scales, we deduce their order in v . Start with the normalization of a scalar current:

$$\langle M | \int d^3x h^\dagger(x) h(x) | M \rangle \sim 1 \quad (2.86)$$

where $|M\rangle$ is some heavy meson state. Since we expect the meson state to be localized in a region of size $1/p$, we can assert that

$$\int d^3x \sim \frac{1}{p^3} \quad (2.87)$$

from this and (2.86), we find $h \sim p^{3/2} \sim v^{3/2}$. The order of the derivative operator can be deduced from

$$E_K = \langle M | \int d^3x h^\dagger(x) \frac{D^2}{2M} h(x) | M \rangle \quad (2.88)$$

to be $D \sim v$. Following such a chain of arguments, we can deduce the order in v of any operator.

- The Lagrangian to $\mathcal{O}(v^n)$ is then simply all of the operators satisfying the symmetries of *QCD* of orders below v^n , with some Wilson coefficients [50]. To $\mathcal{O}(v^6)$:

$$\begin{aligned} \mathcal{L}_{\text{NRQCD}} = & h^\dagger \left(iD_0 + \frac{\mathbf{D}^2}{2m} + c_1 \frac{\mathbf{D}^4}{m^3} + c_2 g \frac{\mathbf{D} \cdot \mathbf{E} - \mathbf{E} \cdot \mathbf{D}}{m^2} \right. \\ & + c_3 ig \frac{\sigma \cdot (\mathbf{D} \times \mathbf{E} - \mathbf{E} \times \mathbf{D})}{m^2} + c_4 g \frac{\sigma \cdot \mathbf{B}}{m} \\ & + f_1 g \frac{\{\mathbf{D}^2, \sigma \cdot \mathbf{B}\}}{m^3} + f_2 ig \frac{\{\mathbf{D}^2, \sigma \cdot (\mathbf{D} \times \mathbf{E} - \mathbf{E} \times \mathbf{D})\}}{m^4} + f_3 ig^2 \frac{\sigma \cdot \mathbf{E} \times \mathbf{E}}{m^3} \Big) h \\ & + d_1 \frac{(h^\dagger H)(H^\dagger h)}{m^2} + d_2 \frac{(h^\dagger \sigma H) \cdot (H^\dagger \sigma h)}{m^2} \\ & + d_3 \sum_a \frac{(h^\dagger T^a H)(H^\dagger T^a h)}{m^2} + d_4 \sum_a \frac{(h^\dagger T^a \sigma H) \cdot (H^\dagger T^a \sigma h)}{m^2} \end{aligned} \quad (2.89)$$

\mathbf{E} and \mathbf{B} are the chromoelectric and chromomagnetic fields, T^a are *SU(3)* color generators, and H is the antiquark components of the heavy quark. $c_{1,2,3,4}, f_{1,2,3}, d_{1,2,3,4}$ are Wilson coefficients, to be fixed by perturbative matching to full QCD at the cutoff (the heavy quark mass, where QCD is perturbative), then the coefficients can be run down to the scale of interest.

CHAPTER 3

Lattice Quantum Chromodynamics

As discussed in sec. 2.3.1, at low energies ($\sim 200\text{MeV}$ and below), QCD becomes non-perturbative. In other words, the coupling α_s becomes $\mathcal{O}(1)$, and an expansion in α_s (as in perturbation theory) will not be dominated by the leading orders. In order to calculate observables of low energy QCD (like hadronic form factors), we require an alternative to perturbation theory.

The expectation value of an observable \mathcal{O} in a Yang-Mills theory can be expressed as a path integral;

$$\langle \mathcal{O} \rangle = \frac{1}{Z} \int [dG d\psi d\bar{\psi}] \mathcal{O} e^{iS[G, \psi, \bar{\psi}]}, \quad (3.1)$$

where A is a gauge field, $\psi(\bar{\psi})$ is an (anti)fermion field, S is the classical action, and $[dG d\psi d\bar{\psi}]$ denotes integration over all configurations of the gauge and fermion fields. $Z = \langle 1 \rangle$ is the partition function. In the perturbative approach, we would expand $\exp(-\text{interacting part of } S)$ resulting in a power series in the gauge coupling populated by Feynman diagrams.

The other option is to instead carry out the integral directly, by numerical brute force. Since it is not numerically feasible to carry out an infinite number of integrals, one must approximate spacetime as a discrete 4 dimensional lattice with spacing " a " between lattice sites, finite spacial volume L_x^3 and finite temporal extent L_t . The functional integral becomes

$$\int [dG d\psi d\bar{\psi}] \rightarrow \prod_n \int dU(x_n) d\psi(x_n) d\bar{\psi}(x_n), \quad (3.2)$$

where n is a 4-vector with integer components labelling the sites, and $x_n^\mu = an^\mu$. This has a second benefit which is to naturally regularize the theory with a momentum cutoff $\Lambda \sim 1/a$. The gauge field has been replaced with the *gauge link* U , to be defined in the following section.

To avoid having to integrate over imaginary numbers (more specifically to avoid the scourge of the *sign problem* [51]), one also performs a *Wick rotation*. This is the redefinition $t \rightarrow it$, which changes the metric from Minkowski to Euclidean, and changes the weight $\exp iS \rightarrow \exp -S$. This has the advantage that it turns the quantum path integral into simply an average in statistical mechanics, this means we can apply all of the machinery of statistical mechanics to computing expectation values.

To obtain the 'real world' result for some expectation value, where the real world means $a = 0$, one must perform the path integral at a number of different a values, and then extrapolate the results to $a = 0$.

One must choose a discretized version of the QCD action S , one which becomes continuum QCD in the continuum ($a \rightarrow 0$) limit. This is a far from trivial step. There are an infinite number of choices of lattice actions that become QCD in the continuum limit. There therefore is a huge literature of different choices of discrete lattice actions. Different collaborations use different actions, and there is never-ending argument about the merits and pitfalls of each.

The rest of this chapter is dedicated to motivating and detailing the choices of discretisation used in the work of this thesis.

3.1 Lattice Gauge Fields

Often the best way to introduce some sophisticated method or technique is to first show how the naive approach breaks down. Imagine attempting a naive discretisation of the QCD action. Derivatives can be replaced with something like

$$\partial_\mu f(x) \rightarrow \frac{1}{2a} (f(x + a\hat{\mu}) - f(x - a\hat{\mu})) \quad (3.3)$$

where $\hat{\mu}$ is the unit vector in the μ direction. The quark kinetic part of the QCD action, $\bar{q}\not{D}q$, becomes

$$\frac{1}{2a} \bar{q}(x)\gamma^\mu q(x + a\hat{\mu}) - \frac{1}{2a} \bar{q}(x)\gamma^\mu q(x - a\hat{\mu}) - ig\bar{q}(x)G_\mu(x)\gamma^\mu q(x). \quad (3.4)$$

This is no longer invariant under the gauge trasforms (2.45), for example the first term becomes $\bar{q}(x)\Lambda(x)^\dagger\Lambda(x + a\hat{\mu})(x + a\hat{\mu})$. The finite difference between lattice sites force us to think more carefully about the interpretation of gauge symmetry on a lattice.

Formally speaking, a gauge feild is a connection on a fibre bundle. We will flesh out what this means.

At each point x , there is a space of possible vectors that a quark field $q(x)$ could be, call it V_x . In this case, this is the colour space, the space of colour vectors (this refers to a single flavour, we suppress the flavour index here for breifity). These spaces are called *fibres*. Spacetime, in our case \mathbb{E}^4 , is called the *base space* in this context.

The problem with our non-gauge-invariant terms above is that we are trying to compare vectors in different fibres. To compare colour vectors at two different spacetime points, i.e. two different fibres, one must *parallel transport* the vector from one point to another, according to some rule of how it changes, the so-called *connection*. In our case the parallel transport is a Wilson line:

$$\begin{aligned} W(x, y) : V_y &\rightarrow V_x \\ W(x, y) &= Pe^{ig \int dc \cdot G} \end{aligned} \quad (3.5)$$

where c is some curve between x and y , and P orders the operation of the gauge field G on the fibres, i.e. the G . A wilson line transforms under the gauge group like $W(x, y) \rightarrow \Lambda(x)W(x, y)\Lambda^\dagger(y)$, so operators like $\bar{q}(x)W(x, y)q(y)$ are gauge-invariant, reflecting the fact that the color vector $q(y)$ has been parallel transported into the same fibre as $\bar{q}(x)$.

From this we see that, on a lattice, the natural degrees of freedom are no longer the elements of the Lie algebra, G_μ , but Wilson lines connecting adjacent lattice sites, also known as *links*:

$$U_\mu(x) : V_x \rightarrow V_{x+a\hat{\mu}}, \in SU(N_c) \quad (3.6)$$

that Gauge transform like

$$U_\mu(x) \rightarrow \Lambda(x)U_\mu(x)\Lambda^\dagger(x + a\hat{\mu}). \quad (3.7)$$

Then, a bilinear of colour vectors at any two points can be made to be gauge invariant by including a path between them made of links. For example;

$$\begin{aligned} \bar{q}(x)U_\mu(x)q(x + a\hat{\mu}) &\rightarrow [\bar{q}(x)\Lambda^\dagger(x)](\Lambda(x)U_\mu(x)\Lambda^\dagger(x + a\hat{\mu}))[\Lambda(x + a\hat{\mu})q(x + a\hat{\mu})] \\ &= \bar{q}(x)U_\mu(x)q(x + a\hat{\mu}). \end{aligned} \quad (3.8)$$

The $\bar{q}\not{D}q$ term in the QCD Lagrangian can then be represented on the lattice in a Gauge invariant way by

$$\frac{1}{2a}\bar{q}(x)\gamma_\mu(U_\mu(x)q(x + a\hat{\mu}) + U_\mu^\dagger(x - a\hat{\mu})q(x - a\hat{\mu})) \quad (3.9)$$

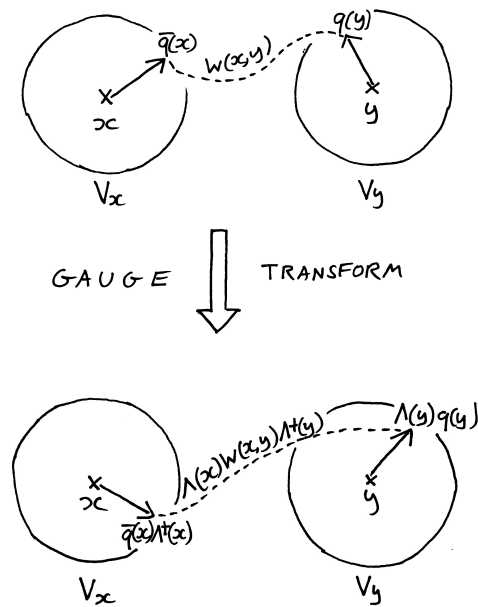


Figure 3.1: Depiction of colour spaces (fibres) at two points in spactime (base space) with the value of the quark field q represented at each point as a colour vector, and the connection $W(x,y)$ needed to compare the two colour vectors. A gauge transform changes the two vectors in different ways, for the comparison to be gauge independent, the connection must also transform appropriately.

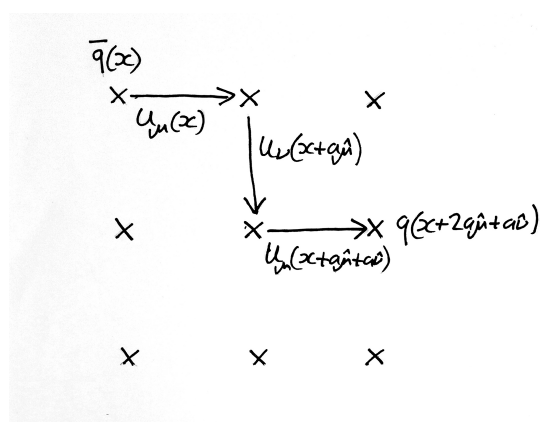


Figure 3.2: Depiction of a gauge invariant quark bilinear, connected by a Wilson line made of gauge links.

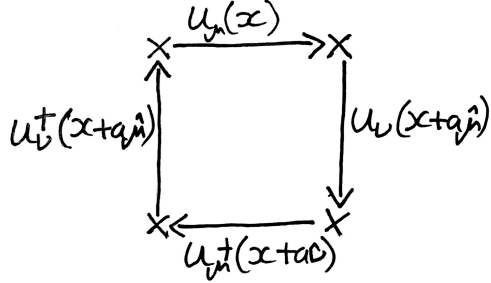


Figure 3.3: Elementary Plaquette.

If one defines the links in terms of the continuum gauge fields G_μ via

$$U_\mu(x) = \exp \left(ig a G_\mu \left(x + \frac{a\hat{\mu}}{2} \right) \right), \quad (3.10)$$

then (3.9) takes the correct form in the continuum limit, i.e. it becomes $\bar{q}Dq + \mathcal{O}(a^2)$.

3.1.1 The Gauge Action

We must design a pure gauge part of the action in terms of link variables. It is clear that the only pure-gauge operators, operators depending only on the link variables, are closed loops of links, as in fig. 3.3.

This brings us basically all the way to the correct answer. The simplest lattice discretisation of the Yang-Mills action is the real part of the smallest possible closed loop of gauge links;

$$S_G = -\frac{1}{g^2} \sum_x \sum_{\mu \neq \nu} \text{Re} \text{Tr}(1 - \square_{\mu\nu}(x)), \quad (3.11)$$

$$\square_{\mu\nu} = U_\mu(x)U_\nu(x + a\hat{\mu})U_\mu^\dagger(x + a\hat{\nu})U_\nu^\dagger(x). \quad (3.12)$$

$\square_{\mu\nu}$ is called the *elementary plaquette*. In the continuum limit this action reduces to

$$S_G = \frac{1}{4} \int d^4x \text{Tr}G_{\mu\nu}G^{\mu\nu} + \mathcal{O}(a^2) \quad (3.13)$$

as required.

This lattice action has a sensible interpretation in terms of the geometrical interpretation of gauge theory. The gauge force is due to *curvature* in the gauge field, which is essentially a path-dependence in parallel transport. If the parallel transport

of a colour vector between x and y was dependent on the path taken between x and y , this is said to be the presence of curvature. The gauge force is due to the presence of curvature, and the simplest local measure of the curvature is the plaquette.

In fact, any closed loop reduces to the Yang-Mills action in the continuum. This can be seen intuitively, taking the continuum limit means shrinking any closed loop into an infinitesimally small point. We then have a choice of gauge action on the lattice.

3.1.2 Symmanzik Improvements of the Gauge Action

As mentioned in the last section, any lattice action is admissible for a calculation as long as it reduces to the appropriate QCD action in the continuum. This gives us a lot of freedom in how we chose our lattice action. A pure gauge action can be any combination of closed Wilson loops.

This freedom can be exploited in order to push observables on the lattice closer to their continuum values (reduce the 'discretisation effects'), such that if one needed to perform an extrapolation of some expectation value to continuum, the extrapolation would be better controlled. This program is known as *Symmanzik improvement*.

In general, a sensible lattice action looks like

$$S = \sum_i c_i(g) \mathcal{O}_{\text{lat}}^i = z_0(\{c_i\}) S_{\text{cont}} + a^2 \sum_{n=1} z_n(\{c_i\}) S_n \quad (3.14)$$

where S_{cont} is the continuum action. We are free to choose any $\{c_i\}$ such that $z_0(\{c_i\}) = 1$. In every example we are concerned with $\mathcal{O}(a)$ terms are absent, hence we have ignored that possibility here. A fundamental postulate of the Symmanzik approach is that improvement (removal of discretisation effects) of one observable results in improvement of all other observables. With this in mind, a reasonable approach is:

- Choose some set of lattice operators $\{\mathcal{O}_{\text{lat}}^i\}$. The number of operators required can be deduced by looking at the number of allowed irrelevant operators in the continuum theory at the mass dimension of the order of a you want to remove, i.e. the number of S_n operators in (3.14).
- Inspect continuum limit of lattice action to find $z_0(\{c_i\})$, enforce $z_0(\{c_i\}) = 1$.
- Choose some observable \mathcal{O} that can be calculated in both the lattice and continuum theory. Use the remaining freedom in $\{c_i\}$ to remove the leading a

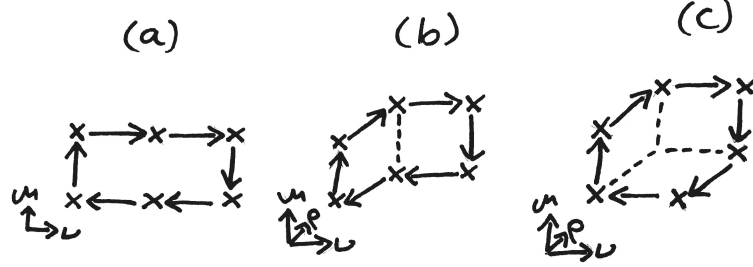


Figure 3.4: Terms additional to the elementary plaquette in the improved pure QCD action.

dependence in $\langle \mathcal{O} \rangle$ order by order in perturbation theory. i.e., if we write the expectation value as

$$\langle \mathcal{O} \rangle = \sum_{n,m} a^{2n} g^{2m} \langle \mathcal{O}_{n,m}(\{c_i\}) \rangle, \quad (3.15)$$

then this amounts to demanding that $\langle \mathcal{O}_{1,m}(\{c_i\}) \rangle = 0$, for as many m 's as possible.

Applying this to pure QCD, this procedure results in the Lüscher-Weitz action [52], we will outline the process here. First consider the number of operators required. In continuum pure QCD, the only dimension 4 operator is $\text{Tr}G_{\mu\nu}G^{\mu\nu}$. There are no dimension 5 operators, hence there can be no $\mathcal{O}(a)$ contribution to the continuum limit of a lattice action. There are three independent dimension 6 operators:

$$\begin{aligned} S_1 &= \text{Tr}J_{\mu\nu\rho}J_{\mu\nu\rho} \\ S_2 &= \text{Tr}J_{\mu\mu\rho}J_{\nu\nu\rho} \quad J_{\mu\nu\rho} = [D_\mu, G_{\nu\rho}] \\ S_3 &= \text{Tr}J_{\mu\mu\nu}J_{\mu\mu\nu} \end{aligned} \quad (3.16)$$

Hence we require 3 extra operators in the lattice action to be tuned in order to remove the three contributions from the a^2 terms in (3.14). The simplest choice is to take the plaquette action (3.12), and add all possible Wilson loops containing 6 links. This set consists of three families related by hypercubic invariance, *rectangles* (a), *parallelograms* (b) and *chairs* (c), depicted in fig. 3.4.

So the new lattice action is

$$S_G = -\frac{1}{g^2} \sum_x \sum_{\mu \neq \nu} (-c_0(g) \operatorname{Re} \operatorname{Tr}(1 - \square_{\mu\nu}(x)) + c_1(g) \operatorname{Re} \operatorname{Tr}(1 - \square_{\mu\nu}^a(x))) \quad (3.17)$$

$$+ \sum_{\rho \neq \mu, \nu} (c_2(g) \operatorname{Re} \operatorname{Tr}(1 - \square_{\mu\nu\rho}^b(x)) + c_3(g) \operatorname{Re} \operatorname{Tr}(1 - \square_{\mu\nu\rho}^c(x))) \quad (3.18)$$

where $\square_{\mu\nu(\rho)}^{a,b,c}$ are the Wilson loops in fig. 3.4. Expanding this in small a , one finds the function $z_0(\{c_i\})$, setting this to one we find the condition [53];

$$c_0 + 8(c_1 + c_2) + 16c_3 = 1. \quad (3.19)$$

The rest of the freedom must be fixed by comparing observables in the lattice and continuum theories. In [54] for example, by matching the gluon propagator between the two theories, one constrains the coefficients further (at tree level)

$$c_1 = -\frac{1}{12}, \quad c_0 - 8c_3 = \frac{5}{3} \quad (3.20)$$

These are classical relations, so will only prevent lattice artifacts up to $\mathcal{O}(\alpha_s)$. For better improvement, one must compare observables that are sensitive to loop corrections. A popular choice of observable is the so-called static quark potential $V(L)$. This is the potential energy between two static colour charges, as a function of separation aL between them. It can be related to the expectation value of a rectangular Wilson loop $\square(L, T)$, extending in one spacial direction by L links and in the time direction by T links. In the $T \rightarrow \infty$ limit, this can be written as

$$\langle \operatorname{Re} \operatorname{Tr} \square(L, T) \rangle \propto \int [d\psi d\bar{\psi} dU] e^{-\sum_x \mathcal{L} + igaA_0\delta_{\mathbf{x}, \mathbf{x}_0} - igaA_0\delta_{\mathbf{x}, \mathbf{x}_1}} \quad (3.21)$$

where $\mathbf{x}_0, \mathbf{x}_1$ are two spacial indices L links apart. This can be interpreted as the partition function Z in the presence of two (oppositely charged) static colour charges at \mathbf{x}_1 and \mathbf{x}_2 . From statistical mechanics, the partition function is related to the internal energy of the system via $E = -\frac{1}{T} \ln Z$. This motivates the expression for the static quark potential:

$$V(L) = -\lim_{T \rightarrow \infty} \frac{1}{T} \ln \left(\frac{1}{N} \langle \operatorname{Re} \operatorname{Tr} \square(L, T) \rangle \right), \quad (3.22)$$

where aN is the spacial extent of the lattice. To constrain $\{c_i\}$, one evaluates this order by order in perturbation theory from the continuum and lattice theories, this amounts to comparing $w_n(L, T)$ from the two theories where this is defined by

$$-\ln \left(\frac{1}{N} \langle \operatorname{Re} \operatorname{Tr} \square(L, T) \rangle \right) = \sum_{n=1}^{\infty} \frac{g_0^{2n}}{(2n)!} w_n(L, T). \quad (3.23)$$

This procedure is effected by the presence of fermions, so it has been performed a number of times to accomodate different fermion discretisations. In this thesis we report results using the Lüscher-Weitz action for gauge fields and HISQ fermions (see sec. 3.2). In this context, the coefficients $\{c_i\}$ were fixed at one-loop via $w_1(L, T)$ in [55], to be

$$c_0 = \frac{5}{3} + (0.237088(46) - 0.1008(34)N_f)\alpha_s + \mathcal{O}(\alpha_s^2) \quad (3.24)$$

$$c_1 = -\frac{1}{12} + (-0.025218(4) + 0.0110(3)N_f)\alpha_s + \mathcal{O}(\alpha_s^2) \quad (3.25)$$

$$c_2 = 0 + (-0.025218(4) + 0.0110(3)N_f)\alpha_s + \mathcal{O}(\alpha_s^2) \quad (3.26)$$

$$c_3 = 0 \quad (3.27)$$

since these have been tuned to remove a^2 effects up to α_s , lattice artifacts in observables computed using this action will be of size $\mathcal{O}(a^2\alpha_s^2)$, so we say this action is $\mathcal{O}(a^2\alpha_s)$ -improved.

3.2 Lattice Fermions

Putting fermions on the lattice supply a much larger host of complications than gauge fields do. There exist a diverse array of approaches to dealing with fermions on the lattice adopted by different collaborations. Different actions are suited to different types of applications, and intense debates have taken place over the years about the theoretical grounding of various actions. The plethora of fermion actions is due mostly to the famous doubling problem, which we will describe below.

In this chapter we will focus only on the fermion actions used in this work; namely the Highly Improved Staggered Quark (HISQ) action, and the Non-Relativistic QCD (NRQCD) action.

Before beginning the discussion of fermion discretisations, we will define some common notation used for gamma matrcies in this context. We are interested in studying theories in Euclidean space, so we will use euclidean gamma matrices, obeying

$$\{\gamma_\mu, \gamma_\nu\} = 2\delta_{\mu\nu}. \quad (3.28)$$

These have the useful property $\gamma_\mu^2 = 1$. The full set of spin-mixing matrices can be labelled according to

$$\gamma_n = \prod_\mu (\gamma_\mu)^{n_\mu} \quad n_\mu = \mathbb{Z}_2 \quad (3.29)$$

There are 16 such matrices representing corners of the hypercube. One can also use a general site vector x_μ to label the matrix, then $\gamma_x = \gamma_n$ where $n_\mu = x_\mu/a \bmod 2$. One can show that for any n ; $\gamma_n^\dagger \gamma_n = 1$. We also define $\gamma_{5\mu} = i\gamma_5 \gamma_\mu$, and $\gamma_{5n} = \prod_\mu (\gamma_{5\mu})^n$.

3.2.1 The Naive Fermion Action & The Doubling Problem

The interacting Dirac action is most naively discretised with

$$S_F = \sum_{x,\mu} \bar{\psi}(x) \gamma_\mu \nabla_\mu \psi(x) + m \sum_x \bar{\psi}(x) \psi(x), \quad (3.30)$$

where ∇_μ is the gauge covariant finite difference operator,

$$\nabla_\mu \psi(x) = \frac{1}{2a} \left(U_\mu(x) \psi(x + a\hat{\mu}) - U_\mu^\dagger(x - a\hat{\mu}) \psi(x - a\hat{\mu}) \right). \quad (3.31)$$

S_F is invariant under a so-called “doubling symmetry”, which is generated by

$$\psi(x) \rightarrow \mathcal{B}_\mu \psi(x) \equiv (-1)^{x_\mu/a} \gamma_{5\mu} \psi(x) \quad (3.32)$$

$$\bar{\psi}(x) \rightarrow \bar{\psi}(x) \mathcal{B}_\mu^\dagger \equiv (-1)^{x_\mu/a} \bar{\psi}(x) \gamma_{5\mu}^\dagger. \quad (3.33)$$

The product space of these form a group of 16 elements $\{\mathcal{B}_\zeta\}$, labeled by vectors ζ with $\zeta_\mu \in \mathbb{Z}_2$ (e.g. the element $\mathcal{B}_0 \mathcal{B}_1$ is labeled by $\zeta = (1, 1, 0, 0)$).

The physical significance of this symmetry can be seen when we study its effect on the action. First, notice that

$$\mathcal{B}_\mu \psi(x) = \gamma_{5\mu} \sum_k \tilde{\psi}(k) e^{i(k + \frac{\pi}{a}\hat{\mu}) \cdot x} \quad (3.34)$$

$$= \gamma_{5\mu} \sum_k \tilde{\psi}(k - \frac{\pi}{a}\hat{\mu}) e^{ik \cdot x}, \quad (3.35)$$

where $\{k\}$ is a discrete set of 4-momenta, with k_μ values spaced by $\pi/a N_\mu$ (N_μ = number of sites in direction μ) and truncated at π/a , due to finite size and finite lattice spacing. The action in momentum space can be written as

$$S = \sum_k \bar{\tilde{\psi}}(k) M(k) \tilde{\psi}(k). \quad (3.36)$$

After the operation of \mathcal{B}_μ it becomes

$$S \rightarrow \sum_k \bar{\tilde{\psi}}(k) \gamma_{5\mu} M(k + \frac{\pi}{a}\hat{\mu}) \gamma_{5\mu} \tilde{\psi}(k) \quad (3.37)$$

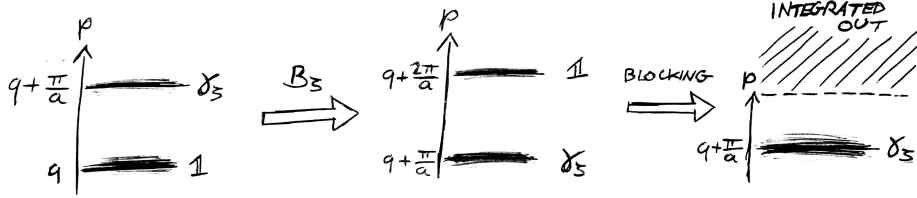


Figure 3.5: Illustration of isolating a single taste via a doubling symmetry transformation \mathcal{B}_ζ then a block-scaling.

Since we know S is invariant under this transformation, it must be true that $\gamma_{5\mu} M(k + \frac{\pi}{a} \hat{\mu}) \gamma_{5\mu} = M(k)$, and therefore

$$M^{-1}(k + \frac{\pi}{a} \hat{\mu}) = \gamma_{5\mu} M^{-1}(k) \gamma_{5\mu} \quad (3.38)$$

M^{-1} is the momentum space propagator for the fermion field, so 3.38 shows that the spectrum of the fermion is periodic, with a period of π/a . We expect a pole in $M^{-1}(k)$ where $k \sim m$, where m is the pole mass of the fermion, but there will now be a second pole at $m + \pi/a$. This will be around the natural cutoff imposed by the lattice $1/a$, and any higher poles like $m + 2\pi/a$ is far above the cutoff so will not contribute.

Generalizing this argument to all elements of the doubling symmetry, we see that

$$M^{-1}(k + \frac{\pi}{a} \zeta) = \gamma_{5\zeta} M^{-1}(k) \gamma_{5\zeta}. \quad (3.39)$$

This leads to 16 poles in the fermion spectrum, one for each *zeta* choice, therefore 16 distinct excitations (called *tastes*).

One can isolate a single taste by a block-scaling procedure;

$$\psi^{(\zeta)}(x_B) = \frac{1}{16} \sum_{\delta x_\mu \in \mathbb{Z}_2} \mathcal{B}_\zeta(x_B + \delta x) \psi(x_B + \delta x). \quad (3.40)$$

For example, for $\zeta = 0$, it would only contain the original non-doubler taste, since all other poles at $|k| \sim \pi/a$ have been integrated out. For $\zeta \neq 0$, the \mathcal{B}_ζ operator pushes the ζ doubler to where the $\zeta = 0$ taste originally was in k space, then the blocking procedure integrates out the rest.

3.2.2 Staggered Quarks

There are a number of solutions to this problem. The most straightforward is to modify the action to push the mass of the unwanted tastes above the momen-

tum cutoff, preventing it from influencing the dynamics, these are called *Wilson-type fermions* [56]. However, actions of this type explicitly break Chiral symmetry. Among other issues, this causes additive renormalization of the fermion mass, immensely complicating renormalization procedures.

Another approach, known as *staggered fermions* [57], partially resolves the doubling issue while retaining chiral symmetry (?). The work presented in this thesis makes extensive use of the staggered formalism.

Staggered fermions are defined via the following. Redefine the fields according to

$$\psi(x) = \gamma_x \chi(x). \quad (3.41)$$

In terms of the new spinor variables $\chi(x)$, the naive action (3.30) becomes

$$S_F = \bar{\chi}(x)[\alpha_\mu(x)\nabla_\mu + m]\chi(x) \quad (3.42)$$

where $\alpha_\mu(x) = (-1)^{\sum_{\nu < \mu} x^\mu/a}$. The action is now diagonal in spin, leading to 4 decoupled grassman variables with identicle actions and identicle coupling to the gauge field. As a result, χ propagators (on fixed gauge backgrounds) are spin diagonal:

$$M_\chi^{-1}(x, y)[U] = g(x, y)[U] \mathbf{1}_{\text{spin}}, \quad (3.43)$$

where $g(x, y)$ is a singlet under spin. One need only to include a single component of χ in a simulation (i.e. fix $\chi = (\chi_1, 0, 0, 0)$). Then they can compute $M_\chi^{-1}(x, y)[U]$ to obtain $g(x, y)$. Then, using the inverse of (3.41), $g(x, y)$ can be transformed to a propagator of the original spinors:

$$M_\psi^{-1}(x, y)[U] = g(x, y)[U] \gamma_x \gamma_y^\dagger. \quad (3.44)$$

This is clearly computationally beneficial. But also, by shaving off the other spinor components, one reduces the number propagating degrees of freedom by a factor of 4, cutting the number of tastes from 16 down to 4.

We can show more explicitly how this happens. To do this, consider rewriting an isolated taste (3.40) in the staggered formalism, i.e., in terms of χ ;

$$\psi^{(\zeta)}(x_B) = \frac{1}{16} \sum_{\delta x_\mu \in \mathbb{Z}_2} \gamma_{\delta x} \mathcal{B}_\zeta(0) \chi(x + \delta x). \quad (3.45)$$

Recall we set $\chi(x) = (\chi_1(x), 0, 0, 0)$. The product $\gamma_{\delta x} \mathcal{B}_\zeta(0)$ is simply a product of gamma matrices, so can only serve to “scramble” the elements of χ . Then, in the

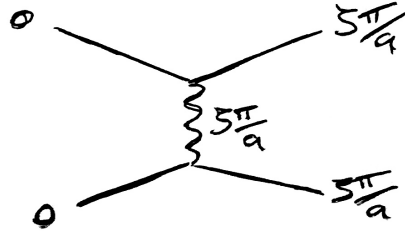


Figure 3.6: Taste mixing at tree level.

staggered formalism, all 16 tastes $\psi^{(\zeta)}$ amount to only 4 distinguishable fermions: $(\chi_1, 0, 0, 0)$, $(0, \chi_1, 0, 0)$, $(0, 0, \chi_1, 0)$, $(0, 0, 0, \chi_1)$ (with factors of (-1) and i).

In practice in lattice calculations, the remaining multiplicity is tacked in 3 steps:

1. Ensure only one taste is created and destroyed in the propagator.
2. Minimize the interaction between tastes by a modification of the action.
3. Remove contributions of extra tastes in the sea by taking $\det M \rightarrow \sqrt[4]{\det M}$
(the context required to understand this step is elucidated in chapter 4).

The third step is the main source of objection to using the staggered formalism for lattice calculations. We will briefly explain this contention in chapter 4.

3.2.3 Highly Improved Staggered Quarks

Step 2 above is the guiding principle for the action we in much of this work, the Highly Improved Staggered Quark action (HISQ) [58].

Interaction between different tastes ("taste mixing") is dominated by the process in fig. 3.6, the exchange of single gluons carrying momenta close to $\zeta\pi/a$. In HISQ, this is suppressed by modifying the gauge fields in such a way as to minimize the coupling between a gluon with momentum $\zeta\pi/a$ and the fermions, in other words, minimize the vertices in fig. 3.6.

To this end, one can change the action so that fermions only couple to *smeared* gauge links, in which high frequency excitations have been removed. Define the first

and second covariant derivative operators;

$$\begin{aligned} \delta_\rho U_\mu(x) &\equiv \frac{1}{a} \left(U_\rho(x) U_\mu(x + a\hat{\rho}) U_\rho^\dagger(x + a\hat{\mu}) \right. \\ &\quad \left. - U_\rho^\dagger(x - a\hat{\rho}) U_\mu(x - a\hat{\rho}) U_\rho(x - a\hat{\rho} + a\hat{\mu}) \right) \end{aligned} \quad (3.46)$$

$$\begin{aligned} \delta_\rho^{(2)} U_\mu(x) &\equiv \frac{1}{a^2} \left(U_\rho(x + a\hat{\rho}) U_\rho^\dagger(x + a\hat{\mu}) \right. \\ &\quad \left. - 2U_\mu(x) \right. \\ &\quad \left. + U_\rho^\dagger(x - a\hat{\rho}) U_\mu(x - a\hat{\rho}) U_\rho(x - a\hat{\rho} + a\hat{\mu}) \right). \end{aligned} \quad (3.47)$$

With this we can define the smearing operator;

$$\mathcal{F}_\mu = \prod_{\rho \neq \mu} \left(1 + \frac{a^2 \delta_\rho^{(2)}}{4} \right) \quad (3.48)$$

HISQ uses two different smeared gauge fields defined by

$$X_\mu(x) \equiv \mathcal{U} \mathcal{F}_\mu U_\mu(x), \quad (3.49)$$

$$W_\mu(x) \equiv \left(\mathcal{F}_\mu - \sum_{\rho \neq \mu} \frac{a^2 (\delta_\rho)^2}{2} \right) \mathcal{U} \mathcal{F}_\mu U_\mu(x). \quad (3.50)$$

where \mathcal{U} is a re-unitarization operator, that acts on a matrix A like $\mathcal{U}A = A/\sqrt{A^\dagger A}$.

The HISQ action can then be written as:

$$S_{\text{HISQ}} = \sum_x \bar{\psi}(x) \left(\gamma_\mu \left(\nabla_\mu(W) - \frac{a^2}{6} (1 + \epsilon_{\text{Naik}}) \nabla_\mu^3(X) \right) + m \right) \psi(x) \quad (3.51)$$

Where $\nabla_\mu(Z)$ is the covariant derivative (3.31) with gauge links replaced with Z . This action in fact not only removes tree level interactions like fig. 3.6, but also all taste mixing interactions at 1-loop.

The ∇_μ^3 term is a Symanzik improvement, it reduces the size of discretisation effects of observables computed using this action. The value of ϵ_{Naik} is fixed according to the constraint

$$\lim_{\underline{p} \rightarrow 0} \frac{E^2(\underline{p}) - m^2}{\underline{p}^2} = 1. \quad (3.52)$$

where $E(\underline{p})$ obeys the tree-level dispersion relation from the HISQ action. Tuning ϵ_{Naik} according to this constraint gives us the expression

$$\begin{aligned} \epsilon_{\text{Naik}} &= \frac{4 - \sqrt{4 + 12 \frac{m_{\text{tree}}}{\cosh(m_{\text{tree}}) \sinh(m_{\text{tree}})}}}{\sinh^2(m_{\text{tree}}) - 1}, \\ m_{\text{tree}} &= m \left(1 - \frac{3}{80} m^4 + \frac{23}{2240} m^6 + \frac{1783}{537600} m^8 \right. \\ &\quad \left. - \frac{76943}{23654400} m^{10} \right) + \mathcal{O}(m^{12}). \end{aligned} \quad (3.53)$$

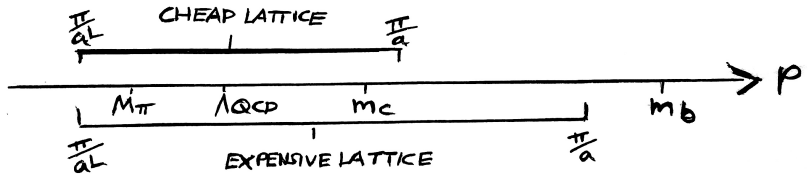


Figure 3.7: Different scales relevant to non-perturbative physics, and brackets showing the range of scales that typical lattices can resolve. The larger the range of scales resolved, the more computationally expensive the calculation.

3.3 Heavy Quarks on the Lattice

The range of different quark masses in nature present a number of further complications to lattice calculations. u and d quarks cause huge problems due to how light they are, this will be addressed in chapter 4. s quarks are easy.

As quarks get heavier, we begin to encounter another problem. Discretisation effects will generally grow like the largest scale in the theory. If the observable being computed on the lattice is sensitive to the dynamics of a heavy quark of mass m_h , this will contain discretisation effects of size $(am_h)^n$ (where n depends on how improved the action is). This is essentially due to the de Broglie wavelength of the heavy quark excitations being close to the lattice spacing, the excitations 'hide' in-between lattice sites.

How heavy we can go is limited to two factors: the improvement of the lattice action and the lattice spacing. How fine we can get the lattice spacing is limited by computational cost. The physical size of the lattice must always be at least large enough to fit the lightest degrees of freedom in the system, namely it must be larger than the wavelength of pions. This means to get smaller lattice spacing requires increasing the number of sites on the lattice, hence increasing the computational costs (details in chapter 4).

In the past, c quarks resulted in uncontrollable discretisation effects, but now armed with highly improved actions like HISQ, and very fine lattices, c physics has been conquered on the lattice [59–65].

The mass of the b is still somewhat out of reach. Even with the HISQ action and the finest lattices available with current computational constraints, physical b quarks will create uncontrollable discretisation effects.

The work in this thesis concerns the decays of mesons containing b quarks. We

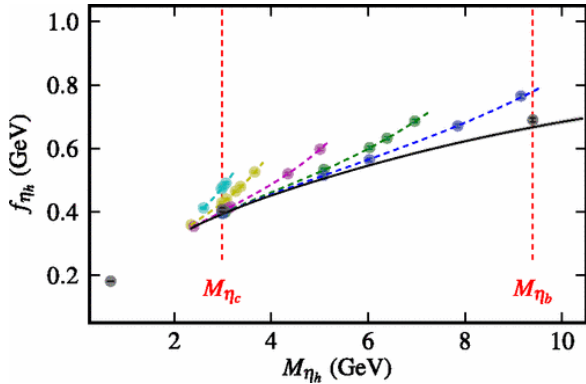


Figure 3.8: An extrapolation to $m_h = m_b$ of the η_h decay constant (where η_h is a pseudoscalar $\bar{h}h$ meson [66]). The colourful points are measurements of f_{η_h} on the lattice, the colour denotes lattice spacing and the x axis, M_{η_h} , is a proxy for the h -quark mass.

approach the issue of the heavy b in two different ways, the *heavy-HISQ* approach, and the *Lattice NRQCD* action. Since the main results of this thesis results from our heavy-HISQ studies, we will not go into too much detail in describing lattice NRQCD.

3.3.1 Heavy HISQ

The heavy-HISQ approach is essentially to model the b with the HISQ action, but to perform the calculation at a number of unphysically light b masses (that we usually refer to generically as heavy h quarks), and extrapolate the results to the physical b mass. Typically the h masses span most of the region between the c mass and the b mass.

Luckily there exists an effective field theory for understanding how to perform such an extrapolation - HQET. HQET gives a framework to describe how observables depend on masses of heavy quarks, so one can use HQET to derive fit forms of such an extrapolation.

The heavy-HISQ approach is a reasonably new program. It has so far been used for computing b decay constants and masses [66], and a number of heavy-HISQ calculations of semileptonic form factors are currently underway. The work presented in chapters 6 and 7 adopt the heavy-HISQ approach. Besides these, there are also calculations of form factors for the $B_c \rightarrow \eta_c l\nu$, $B_c \rightarrow J/\psi l\nu$ [67], $B_c \rightarrow B_s l\nu$, $B_s \rightarrow \eta_s l\nu$, and $B \rightarrow D^* l\nu$ decays.

3.3.2 Lattice NRQCD

The root of the problem of heavy quarks on the lattice is in the rest mass of the quark. Consider the expansion in momentum \mathbf{p}^2 of the continuum relativistic dispersion relation:

$$\omega = \sqrt{\mathbf{p}^2 + m^2} \simeq m + \frac{\mathbf{p}^2}{2m} - \frac{\mathbf{p}^4}{4m^3} + \dots \quad (3.54)$$

the first term (rest mass) is the source of the issue, when $m > 1/a$ the first term pushes the frequency of excitations ω over $1/a$.

Another solution to heavy quarks is to replace the relativistic fermion action e.g. HISQ, with a lattice version of NRQCD [50]. In NRQCD the b has no rest mass.

Another benefit of NRQCD is that it does not suffer from a doubling problem, since the doubling problem is a purely relativistic issue (the doubling symmetry requires 4 component spinors for γ matrices to act on).

The lattice calculations we perform require us to compute propagators for b quarks on fixed gauge backgrounds. The form of the action allows propagators $M^{-1}[U]$ to be computed using a simple recursion relation

$$M_b^{-1}(\mathbf{x}, t+1)[U] = e^{-aH}[U] M_b^{-1}(\mathbf{x}, t)[U] \quad (3.55)$$

which is numerically very fast. In the interest of numerical stability, the time evolution operator is re-cast as

$$e^{-aH} = \left(1 - \frac{a\delta H}{2}\right) \left(1 - \frac{aH_0}{2n}\right)^n U_0^\dagger(\mathbf{x}, t) \left(1 - \frac{aH_0}{2n}\right)^n \left(1 - \frac{a\delta H}{2}\right) \quad (3.56)$$

where n is an arbitrary integer (chosen in our studies to be $n = 4$), and the Hamiltonian has been broken up into a leading part H_0 and correction δH . We use the $\mathcal{O}(\alpha_s v^4)$ corrected NRQCD Hamiltonian:

$$aH_0 = -\frac{\nabla^{(2)}}{2am_b}, \quad (3.57)$$

$$\begin{aligned} a\delta H = & -c_1 \frac{(\nabla^{(2)})^2}{8(am_b)^3} + c_2 \frac{i}{8(am_b)^2} (\nabla \cdot \tilde{\mathbf{E}} - \tilde{\mathbf{E}} \cdot \nabla) \\ & - c_3 \frac{1}{8(am_b)^2} \sigma \cdot (\nabla \times \tilde{\mathbf{E}} - \tilde{\mathbf{E}} \times \nabla) \\ & - c_4 \frac{1}{2am_b} \sigma \cdot \tilde{\mathbf{B}} + c_5 \frac{\nabla^{(4)}}{24am_b} \\ & - c_6 \frac{(\nabla^{(2)})^2}{16n(am_b)^2} \end{aligned} \quad (3.58)$$

where $\nabla^{(2,4)}$ are the second and fourth lattice derivative, $\tilde{\mathbf{E}}$ and $\tilde{\mathbf{B}}$ are the (Symmanzik improved) chromoelectric and chromomagnetic fields. The form of $\nabla^{(2,4)}, \tilde{\mathbf{E}}, \tilde{\mathbf{B}}$ are defined in sec. 4.2 of [50], and were improved upon in [68].

The coefficients $\{c_i\}$ have been fixed via various calculations adopting a number of methods. The coefficients of the kinetic terms, $c_{1,5,6}$, were most recently fixed by comparing the lattice NRQCD dispersion relation to that of the continuum in perturbation theory [69]. c_2 is a spin-independent term which can effect radial and orbital excitation energies, is not expected to have as large an effect as the kinetic terms, so is set to its tree-level value of 1. The result of varying c_2 on relevant observables was investigated in sec. IIIC of [70], and the effects were very small. c_3 and c_4 are spin-dependent terms, which would have a small effect on spin-averaged observables (i.e. all observables computed in this work). c_3 is set to 1, and c_4 is tuned non-perturbatively, by matching predictions of the fine structure of the Υ spectrum from lattice NRQCD to experiment [70].

Once the propagator for the 2-component non-relativistic b quark has been found, it must be transformed back into a 4-component spinor. This is done by the inverse Fouldy-Wouthuysen transformation [49]:

$$\psi(x) = e^{-\frac{\gamma \cdot \nabla}{2m_b}} \begin{pmatrix} \psi_+(x) \\ 0 \end{pmatrix}. \quad (3.59)$$

CHAPTER 4

Lattice Calculations

4.1 Correlation Functions from Lattice Simulations

A typical quantity that is computed on the lattice is a meson correlation function, i.e. when $\mathcal{O} = \Phi(x)\Phi^\dagger(y)$ and Φ is a meson creation operator. This is a good working example for showing the steps in a lattice calculation.

A creation operator for a meson in this context can be any operator containing the same quantum numbers as the meson one is trying to create. For example, the neutral B meson is a pseudoscalar charged with a d and \bar{b} quark, so a suitable operator is $\Phi(x) = \bar{b}(x)\gamma_5 d(x)$. The path integral can then be written as

$$C(x, y) = \int \mathcal{D}\psi \mathcal{D}\bar{\psi} \mathcal{D}U \left(\bar{b}(x)\gamma_5 d(x)\bar{d}(y)\gamma_5 b(y) \right) e^{-S_G[U] - \sum_{w,z} \bar{\psi}(w)M(w,z)[U]\psi(z)} \quad (4.1)$$

where we have now broken the action up into a gauge part $S_G[U]$, and a fermion part. $M(x, y)[U]$ is the Dirac operator, and can be seen as a matrix in lattice site, flavor, color and spin. ψ is a vector of quark flavours.

The integral over fermions can be preformed analytically, since the fermion fields are Grassman valued. In our example, the result is [71],

$$C(x, y) = \int \mathcal{D}U \operatorname{Tr} \left[M_b^{-1}(y, x)[U]\gamma_5 M_d^{-1}(x, y)[U]\gamma_5 \right] e^{-S_G[U]} \det(M[U]) \quad (4.2)$$

The quantities $M_f^{-1}(x, y)[U]$ are propagators of a quark of flavour f on a fixed gauge background U . The integration over gauge fields is generally carried out by an importance sampling method. A finite *ensemble* of gauge configurations $\{U_i\}$ is generated by a Monte Carlo Markov chain (MCMC), where the probability of a gauge configuration U_j being added to the ensemble is proportional to

$$e^{-S_G[U_j]} \det(M[U]) \quad (4.3)$$

See [72] ch. 7 for examples of such algorithms. In the case of our work, we use ensembles generated by the MILC collaboration [73].

Once the ensemble is created, the path integral can be approximated by simply

$$C(x, y) \simeq \frac{1}{N} \sum_i \text{Tr} [M_b^{-1}(y, x)[U_i]\gamma_5 M_d^{-1}(x, y)[U_i]\gamma_5] \quad (4.4)$$

where N is the size of the ensemble. The calculation of the correlation function then is split into 3 steps:

1. Generate an ensemble of Gauge configurations $\{U_i\}$ by MCMC.
2. Compute quark propagators $M_f^{-1}(x, y)[U]$ on each Gauge configuration. This requires inverting the matrix M each time, this is typically done by conjugate gradient method.
3. Construct trace as in (4.4), and average over the ensemble.

We now turn to the issue of choosing lattice actions.

4.1.1 The Path Integral and Generation of Gauge Ensembles

discretise path integral

generate gauge configs using MCMC, breif review of options,
some detail of the option milc uses

4.1.2 Dirac Operator Inversion

conjugate gradient method

mass \simeq condition number \rightarrow light quarks are hard

4.1.3 Staggered Correlation Functions

introduce random wall sources

derive how 2-point functions look in terms of staggered propagators and phases.
similarly for 3-point functions, extended sources.

The full set of spin-mixing matrices can be labelled according to

$$\gamma_n = \prod_{\mu} (\gamma_{\mu})^{n_{\mu}} \quad n_{\mu} = \mathbb{Z}_2 \quad (4.5)$$

There are 16 such matrices representing corners of the hypercube. As $\gamma_\mu^2 = 1$, one can also use a general site vector x_μ to label the matrix, then $\gamma_x = \gamma_n$ where $n_\mu = x_\mu \bmod 2$. One can show that for any x ; $\gamma_x^\dagger \gamma_x = 1$.

Naive quarks $\psi(x)$ can be transformed into staggered quarks $\chi(x)$ via $\psi(x) = \gamma_x \chi(x)$. Then, Naive quark propagators (inverse Dirac operators) become

$$G_\psi(x, y) = \gamma_x \gamma_y^\dagger G_\psi(x, y) \quad (4.6)$$

By conjugating both sides and using γ_5 -hermiticity $G_\psi^\dagger(y, x) = \gamma_5 G_\psi(y, x) \gamma_5$ it can be shown that

$$G_\psi(x, y) = \phi_5(x) \phi_5(y) G_\psi^\dagger(y, x) \quad (4.7)$$

where $\phi_5(x) = (-1)^{\sum_\mu x_\mu}$.

2pt correlation functions

We will break down the correlation function to see what quantities must be computed by the simulation. Consider the generic 2-point correlator:

$$C(x, y) = \langle \Phi_X^\dagger(x) \Phi_Y(y) \rangle_{\psi, U} \quad , \quad \Phi_X(x) = \frac{1}{4} \bar{\psi}_a(x) \gamma_X \psi_b(x) \quad (4.8)$$

$$= \frac{1}{16} \langle \text{tr}_{c,s} \gamma_X G_{a,\psi}(x, y) \gamma_Y G_{b,\psi}(y, x) \rangle_U \quad (4.9)$$

$$= \frac{1}{16} \text{tr}_s \left(\gamma_x^\dagger \gamma_X \gamma_x \gamma_y^\dagger \gamma_Y \gamma_y \right) \langle \text{tr}_c (G_{a,\chi}(x, y) G_{b,\chi}(y, x)) \rangle_U \quad (4.10)$$

tr_s is a trace over spin and tr_c is over colour. To deal with the spin trace, define the family of phases $\{\phi_X(x)\}$ according to

$$\gamma_x^\dagger \gamma_X \gamma_x = \phi_X(x) \gamma_X \quad (4.11)$$

for example, if $X = 5$, then $\gamma_x^\dagger \gamma_5 \gamma_x = (-1)^{\sum_\mu x_\mu} \gamma_x^\dagger \gamma_x \gamma_5 = \phi_5(x) \gamma_5$. The map from X to ϕ_X is structure preserving, i.e. if $\gamma_X = \gamma_A \gamma_B$, then $\phi_X(x) = \phi_A(x) \phi_B(x)$. The spin trace becomes $\phi_X(x) \phi_Y(y) \text{tr}_s(\gamma_X \gamma_Y)$. This will vanish unless $Y = X$, as one would expect physically for the correlation function. We end up with

$$C(x, y) = \frac{1}{4} \phi_X(x) \phi_X(y) \langle \text{tr}_c G_{a,\chi}(x, y) G_{b,\chi}(y, x) \rangle_U \quad (4.12)$$

It is useful in the simulation to replace $G_{b,\chi}(y, x)$ with its conjugate via (4.7), resulting in

$$C(x, y) = \frac{1}{4} \phi_{5X}(x) \phi_{5X}(y) \langle \text{tr}_c G_{a,\chi}(x, y) G_{b,\chi}^\dagger(y, x) \rangle_U \quad (4.13)$$

where $\phi_{5X}(x) = \phi_5(x)\phi_X(x)$. To obtain the correlation function of a meson in an eigenstate with momentum \underline{p} , the above must be replaced with

$$C_{\underline{p}}(t_0, t) = \frac{1}{L^3} \sum_{\underline{x}, \underline{y}} e^{i\underline{p} \cdot (\underline{x} - \underline{y})} C(\underline{x}, t_0; \underline{y}, t) \quad (4.14)$$

$$= \frac{1}{4L^3} \sum_{\underline{x}, \underline{y}} e^{i\underline{p} \cdot (\underline{x} - \underline{y})} \phi_{5X}(x) \phi_{5X}(y) \langle \text{tr}_c G_{a,\chi}(x, y) G_{b,\chi}^\dagger(y, x) \rangle_U, \quad (4.15)$$

where it is understood that $x_0 = t_0$ and $y_0 = t$. In order to evaluate this function, the simulation must perform inversions to create $G_{a/b,\chi}(x, y)$ for each x and y , so $2 \cdot \text{Vol}^2$ operations. This is prohibitively expensive. The number of inversions can be reduced using *random wall sources*. Define

$$P_{a,\underline{p},X}^{t_0}(y) \equiv \frac{1}{\sqrt{L^3}} \sum_{\underline{x}} e^{i\underline{p} \cdot (\underline{x} - \underline{y})} \phi_{5X}(\underline{x}, t_0) \xi(\underline{x}) G_{a,\chi}(\underline{x}, t_0; y), \quad (4.16)$$

where $\xi(\underline{x})$ is a random field of colour vectors, varying with U . This has the property

$$\langle f(\underline{x}, \underline{x}') \xi^*(\underline{x}') \xi(\underline{x}) \rangle_U = \delta_{\underline{x}, \underline{y}} \langle f(\underline{x}, \underline{y}) \rangle_U. \quad (4.17)$$

Using this property it can be shown that the correlator can be build instead according to

$$C(\underline{x}, t_0; \underline{y}, t) \simeq \frac{1}{4} \sum_{\underline{y}} \phi_{5X}(y) \langle \text{tr}_c P_{a,\underline{p},X}^{t_0}(\underline{y}, t) P_{b,0,1}^{t_0,\dagger}(\underline{y}, t) \rangle_U \quad (4.18)$$

Now all the simulation has to do is compute $P_{a/b}^{t_0}(y)$ for general y , so $2 \cdot \text{Vol}$ operations, a reduction by a factor of Vol .

In the MILC code, "sources" are first created (the fields $\phi_{5X}(\underline{x}, t_0) \xi(\underline{x})$), then the objects $P^{t_0}(y)$ (referred to as "propagators") are generated from them. Any extra factors dependant on y (this is useful for "smeared" propagators, see [?](#)) can be multiplied in. The resulting object $f(y) \cdot P^{t_0}(y)$ is referred to as a "quark". Finally, two of these quarks can be "tied together" according to (4.18), to produce correlation functions. The sources are chosen to be on some single timeslice t_0 , resulting in a value for $C(t_0, t)$ at each t .

The above discussion can be generalized to 3- (or N -)point correlation functions using *extended sources*. Consider a 3-pt correlator encoding the form-factors of a semileptonic decay from meson X to meson Z , via a current J . We start by

evaluating

$$\begin{aligned} C(x, y, z) &= \langle \Phi_X^\dagger(x) J(y) \Phi_Z(z) \rangle_{\psi, U} , \quad \Phi_X(x) = \frac{1}{4} \bar{\psi}_b(x) \gamma_X \psi_s(x) \\ J(y) &= \bar{\psi}_b(y) \gamma_J \psi_a(y) \\ \Phi_Z(z) &= \frac{1}{4} \bar{\psi}_a(z) \gamma_Z \psi_s(z) \end{aligned} \quad (4.19)$$

in the same way as before:

$$C(x, y, z) = \frac{1}{16} \text{tr}_s \left(\gamma_x^\dagger \gamma_X \gamma_x \gamma_y^\dagger \gamma_J \gamma_y \gamma_z^\dagger \gamma_Z \gamma_z \right) \langle \text{tr}_c G_{b,\chi}(x, y) G_{a,\chi}(y, z) G_{s,\chi}(z, x) \rangle_U \quad (4.20)$$

$$= \frac{1}{4} \phi_{5X}(x) \phi_J(y) \phi_{5Z}(z) \langle \text{tr}_c G_{b,\chi}(x, y) G_{a,\chi}(y, z) G_{s,\chi}^\dagger(z, x) \rangle_U \quad (4.21)$$

We have assumed that $\text{tr}_s \gamma_X \gamma_J \gamma_Z = 4$, requiring that each gamma matrix in this combination has a partner and therefore cancels. In any other situation the trace would vanish. For example, if the current is a temporal vector $J = 0$, and the two mesons represent pseudoscalars, one of the meson operators must have a γ_0 , i.e. one could choose $\gamma_X = \gamma_0 \gamma_5, \gamma_Z = \gamma_5$. **why is it ok to have a non-goldstone for X ?**

Putting X into an eigenstate of zero momentum, and Y into an eigenstate of momentum \underline{p} , we get

$$C_{\underline{p}}(t_0, t, T) = \frac{1}{4L^3} \sum_{\underline{x}, \underline{y}, \underline{z}} e^{i\underline{p} \cdot (\underline{y} - \underline{z})} \phi_{5X}(x) \phi_J(y) \phi_{5Z}(z) \langle \text{tr}_c G_{b,\chi}(\underline{x}, t_0; \underline{y}, t) G_{a,\chi}(\underline{y}, t, \underline{z}, T) G_{s,\chi}^\dagger(\underline{z}, T; \underline{x}, t_0) \rangle_U \quad (4.22)$$

This can be built by first creating propagators for the b and s quarks: $P_{b,0,X}^{t_0}(y), P_{s,0,1}^{t_0}(z)$. Then, build the a propagator using an extended source, i.e.:

$$P_{a,\underline{p},ext}^T(y) = \sum_{\underline{z}} P_{s,0,1}^{t_0}(\underline{z}, T) \phi_{5Z}(\underline{z}, T) G_{a,\chi}(\underline{z}, T; y) \quad (4.23)$$

Then, by plugging $P_{b,0,X}^{t_0}(y)$ and $P_{a,\underline{p},ext}^T(y)$ into the MILC tie-together defined by (4.18), one ends up evaluating (4.22).

Momentum Twist

The momentum space 2-point correlation function for an operator \mathcal{O} with external momentum \underline{p} is given by

$$C(\underline{p}, t) = \sum_{\underline{x}} e^{i\underline{p} \cdot \underline{x}} \langle \mathcal{O}^\dagger(\underline{x}, t) \mathcal{O}(\underline{0}, 0) \rangle \quad (4.24)$$

To extend the method for computing zero momentum correlators to non-zero, one can compute $S(\underline{0}, t)$ with rephased operators, exploiting the fact that

$$\mathcal{O}(\underline{x}, t) \rightarrow \mathcal{O}(\underline{x}, t)e^{-i\underline{p} \cdot \underline{x}} \quad (4.25)$$

$$\implies C(\underline{0}, t) \rightarrow C(\underline{p}, t) \quad (4.26)$$

This generalised straightforwardly to n -point functions. One can assign the rephasing to any factor in \mathcal{O} , for example a fermion operator

$$\psi(\underline{x}, t) \rightarrow \psi(\underline{x}, t)e^{-i\underline{p} \cdot \underline{x}} \quad (4.27)$$

Rephasing ψ is equivalent to introducing the so-called *momentum twist* to the gauge links. The action of (4.25) on any gauge invariant quantity is equivalent to

$$U_i \rightarrow U_i e^{ip_i} \quad (\text{no sum}) \quad (4.28)$$

proof(ish)

$$\psi^\dagger(x) U_\mu(x) U_\nu(x + \mu) \psi(x + \mu + \nu) \quad (4.29)$$

$$\rightarrow \psi^\dagger(x) U_\mu(x) U_\nu(x + \mu) e^{i(p_\mu + p_\nu)} \psi(x + \mu + \nu) \quad (4.30)$$

$$= \psi^\dagger(x) (e^{ip_\mu} U_\mu(x)) (e^{ip_\nu} U_\nu(x + \mu)) \psi(x + \mu + \nu) \quad (4.31)$$

As an aside, this can be seen as coupling ψ to an additional $U(1)$ gauge field A_μ , with constant value $A_\mu = (0, \underline{p})$ (ref!).

(4.28) is how external momenta is simulated in lattice simulations. In the case of multiple fermion fields, where we want to rephase some and not others (or different repphasings), care must be taken to only give the links a twist when in terms including the appropriate fermion.

4.2 Analysis of Correlation Functions

derive the fit function for correlation functions, 2-point and 3-point
how fit parameters relate to energies, decay constants, transition matrix elements...

4.2.1 Non-Linear Regression

Levenberg-Marquardt algorithm

Bayesian constraining of fits
general rules for priors

Once a correlation function like the in ?? has been computed, we can extract physics from it, namely the mass and decay constant of the meson we are studying. In practice the meson creation operators defined above are fourier transformed

$$\Phi(\underline{k}, t) = \sum_{\underline{x}} e^{-i\underline{k} \cdot \underline{x}} \Phi(\underline{x}, t) \quad (4.32)$$

which serves to change (4.4) into

$$C_{\underline{k}}(t) = \frac{1}{N} \sum_i \sum_{\underline{x}, \underline{y}} e^{-i\underline{k} \cdot (\underline{x} - \underline{y})} \text{Tr} [M_b^{-1}(\underline{y}, t; \underline{x}, 0) [U_i] \gamma_5 M_d^{-1}(\underline{x}, 0; \underline{y}, t) [U_i] \gamma_5] \quad (4.33)$$

(4.33) is computed for many t values with a lattice calculation following the principles detailed above. One performs a least-squares fit of this to a theoretically motivated function of t . To derive such a function, first construct a complete set of momentum \underline{k} states with quantum numbers matching the meson:

$$1 = \sum_{n=0} \frac{1}{2E_n^r} |\lambda_n\rangle \langle \lambda_n|. \quad (4.34)$$

Where $E_n^r = \sqrt{M_n^2 + \underline{k}^2}$ are the relativistic energies of each state. Inserting this into the correlation function, and moving from the Heisenberg to Schrödinger picture;

$$\begin{aligned} C_{\underline{k}}(t) &= \sum_{n=0} \frac{1}{2E_n^r} \langle 0 | e^{Ht} \Phi(\underline{k}, 0) e^{-Ht} | \lambda_n \rangle \langle \lambda_n | \Phi^\dagger(\underline{k}, 0) | 0 \rangle \\ &= \sum_{n=0} \left(\frac{\langle 0 | \Phi(\underline{k}, 0) | \lambda_n \rangle}{\sqrt{2E_n^r}} \right) \left(\frac{\langle \lambda_n | \Phi^\dagger(\underline{k}, 0) | 0 \rangle}{\sqrt{2E_n^r}} \right) e^{-E_n^r t} \\ &\equiv \sum_{n=0} |a_n|^2 e^{-E_n^l t}. \end{aligned} \quad (4.35)$$

The fit results in a determination of the parameters a_n , and E_n^l . Since the lowest energies dominate the function at late times, one can afford to truncate the sum over n to some tractable range, in our case $n \in [1, 6]$. We interpret $|\lambda_0\rangle$ to be the ground state of the meson we are studying. The exponential decays mean the fit function is dominated by the ground state at large t , and subsequent excited states

become less important as E_n^l increases. Hence by only including $C_k(t)$ at suitably large t values, we can afford to truncate the sum in n . In our fits we chose $n = 6$.

We maintain a distinction between E^l and E^r , since for example in simulations involving NRQCD quarks these differ. If this is not an issue, as is the case with HISQ, one can compute the correlation function at zero momentum $C_0(t)$, then fit it to find the parameter E_0^l , which will equal the meson's mass M . Noting the definition of a meson decay constant f : $\langle 0|J_0|\text{Meson}(\underline{k}=0)\rangle = Mf$, where J_0 is a temporal current with the same quantum numbers as the meson, we can see that the fit parameters a_n at zero momentum are related to the meson's decay constant via

$$f = \sqrt{\frac{2}{M}} a_0 \quad (4.36)$$

Hence the fit can also be used to extract decay constants.

The above discussion can be straightforwardly generalized to 3-point correlation functions, from which we are able to extract quantities like the hadronic transition amplitudes $H_\mu = \langle M_{q_1\bar{q}_3}|J_\mu^{q_1\bar{q}_2}|M_{q_2\bar{q}_2}\rangle$ from sec. ???. Specifically the quantity we require in order to deduce the $B_s \rightarrow D_s l \nu$ form factors is $\langle D_s|V_\mu|B_s\rangle$, where $V_\mu = \bar{c}\gamma_\mu b$.

The generalization of the above for 3pt functions is summarized here:

$$\begin{aligned} C_3(t, T) &= \int \mathcal{D}\psi \mathcal{D}\bar{\psi} \mathcal{D}U \left(\Phi_{D_s}(0, 0)V_\mu(-\underline{p}, t)\Phi_{B_s}^\dagger(\underline{p}, T) \right) e^{-S[\psi, \bar{\psi}, U]} \\ &\simeq \frac{1}{N} \sum_i \sum_{\underline{x}, \underline{y}, \underline{z}} e^{-i\underline{p} \cdot (\underline{y} - \underline{z})} \text{Tr} \left[M_b^{-1}(\underline{x}, 0; \underline{y}, t)[U_i]\gamma_\mu M_c^{-1}(\underline{y}, t; \underline{z}, T)[U_i]\gamma_5\gamma_5 M_s^{-1\dagger}(\underline{z}, T; \underline{x}, 0)[U_i] \right] \end{aligned} \quad (4.37)$$

$$(4.38)$$

$$\begin{aligned} &= \sum_{n,m} \left(\frac{\langle 0|\Phi_{D_s}|\lambda_n\rangle}{\sqrt{2E_n^r}} \right) \left(\frac{\langle \lambda_n|V_\mu|\lambda_m\rangle}{2\sqrt{E_n^r E_m^r}} \right) \left(\frac{\langle \lambda_m|\Phi_{B_s}^\dagger|0\rangle}{\sqrt{2E_n^r}} \right) e^{-E_m^l(T-t)} e^{-E_n^l t} \\ &\equiv \sum_{n,m} a_{D_s,n} V_{nm} a_{B_s,m}^* e^{-E_m^l(T-t)} e^{-E_n^l t}. \end{aligned} \quad (4.39)$$

$C(t, T)$ is computed at different values of t and T , then a least-squares fit is performed to the fit function (4.40). a_n will vanish for states $|\lambda_n\rangle$ which have different quantum numbers to Φ_{B_s} , and similarly for b_m and Φ_{D_s} . Non-zero a_n 's will match

the analogous parameters extracted from fitting a 2pt function $\langle \Phi_{B_s}^\dagger \Phi_{B_s} \rangle$, similarly for b_n 's and Φ_{D_s} . This carries on to the energies, $\{E_n^l\}$ is the spectrum for the D_s meson, and $\{E_m^l\}$ is the spectrum for the B_s . Therefore, we compute and fit the appropriate 2pt functions to deduce the parameters $\{a_n\}, \{b_m\}, \{E_n^l\}$. Then, fitting $C_3(t, T)$ results in an accurate determination of the remaining free parameters, V_{nm} . This set contains the quantity we need, recognising that:

$$V_{00} = \frac{\langle D_s | V_\mu | B_s \rangle}{2\sqrt{E^{B_s} E^{D_s}}} \quad (4.40)$$

2-point correlation functions are then fitted as in sec. ???. The fit function we use is modified a little from (4.35), we use:

$$\begin{aligned} C^{\alpha\beta}(t) &= \sum_n a_n^{\alpha*} a_n^\beta (e^{-E_n^l t} - s e^{-E_n^l (T-t)}) \\ &\quad + \sum_n a_n'^{\alpha*} a_n'^\beta (-1)^t (e^{-E_n'^l t} - s e^{-E_n'^l (T-t)}) \end{aligned} \quad (4.41)$$

Firstly, the parameters $\{a_n\}$ must vary between source and sink to account for the different operators. Secondly, the periodicity of the lattice in the time direction means an extra exponential term is required, but not in the case of the B_s since NRQCD quarks do not experience the periodicity of the lattice. Hence s is set to 0 for the B_s correlator and 1 for the D_s . T is the time extent of the lattice. The second term is to account for the so-called "oscillating state", which is in fact the $\zeta = (1, 0, 0, 0)$ doubler fermion appearing due to the doubling in the HISQ action (see sec. 3.38). No other doublers contribute, since $\Phi_{\underline{k}}$ has a 3-momentum fixed at \underline{k} , which we always take to be small relative to π/a , hence does not couple to the states at $k \sim (0, \pi/a, 0, 0)$, $k \sim (0, 0, \pi/a, 0)$ etc. However, $\Phi_{\underline{k}}$ can couple to arbitrarily high energy states, so the $k \sim (\pi/a, 0, 0, 0)$ doubler contributes. The second term in (4.41) is justified by performing the doubling operation \mathcal{B}_0 defined in (4.35), the quark fields in $\Phi_{\underline{k}}$ which obey the HISQ action. See appendix G of [58] for details.

We use the *CorrFitter* package [74] for performing Bayesian least-squares fitting to the correlation functions. The package employs the trust region method of least-squares fitting. The fits require priors for each of the fit parameters. The "amplitude" parameters $a_{n, B_s/D_s}^\alpha$ are given priors of 0.1(1.0), thus inserting only the assumption that they are of $\mathcal{O}(1)$. The ground state energies are given priors motivated by the meson masses, and excited state energies are given loose, evenly

spaced priors with 600MeV between each level.

2-point correlation functions for B_s and D_s are fit to (4.41), resulting in $a_{n,B_s/D_s}^\alpha, E_{n,B_s/D_s}^l$. Since the HISQ action is fully relativistic, E_{0,D_s}^l at $\underline{k} = 0$ can be interpreted as the D_s meson mass. The same cannot be done for the B_s . The decay constants for B_s and D_s can be deduced from a_{0,B_s}^0 and a_{0,D_s}^0 , since Φ_{B_s,D_s}^0 are also temporal axial currents. This is a good avenue for consistency checks, we compared M_{D_s}, f_{D_s} and f_{B_s} to those computed in [75], [76] amongst others, and found them to be consistent (modulo small shifts we can reasonably expect due to differing choices of bare quark masses).

We now discuss fitting the 3-point correlation functions. The same considerations as those that went into (4.41) lead us to our 3-point fit function:

$$\begin{aligned} C_3^{\alpha\beta}(t, T) = & \sum_{k,m} \left(a_{k,D_s}^\alpha V_{km}^{nn} a_{m,B_s}^{*\beta} e^{-E_m^l t} e^{-E_k^l (T-t)} \right. \\ & + a_{k,D_s}^\alpha V_{km}^{no} a_{m,B_s}^{'*\beta} e^{-E_m'^l t} e^{-E_k^l (T-t)} \\ & + a_{k,D_s}^{'\alpha} V_{km}^{on} a_{m,B_s}^{*\beta} e^{-E_m^l t} e^{-E_k'^l (T-t)} \\ & \left. + a_{k,D_s}^{'\alpha} V_{km}^{oo} a_{m,B_s}^{'*\beta} e^{-E_m'^l t} e^{-E_k^l (T-t)} \right) \end{aligned} \quad (4.42)$$

The 2-point and 3-point correlators are fit simultaneously, according to fit functions (4.41) and (4.42). The parameters involved in the 2pt fits are mostly fixed by the data in the 2pt correlation functions, so the fit can use most of the data in the 3pt correlation functions to determine the transition amplitudes V_{km}^{ab} . This is carried out for each B_s and D_s smearing, each direction μ and each current correction i of the vector current $V_\mu^{(i)}$.

In this large 2pt/3pt fit, there is a huge χ^2 manifold with many local minima, and it is crucial to impose strong priors in order to ensure the fit finds the true minimum. Priors for ground state 2-point amplitudes and energies $a_{0,B_s/D_s}^\alpha, E_{0,B_s/D_s}^l$ are taken to be the results from individual fits of the 2-point functions, with the errors expanded by a factor of 2. The excited state amplitudes and energies are given the same priors as in the 2-point fits. The transition amplitudes V_{km}^{ab} are given the prior $0.1(1.0)$, assuming it to be $\mathcal{O}(1)$.

Finally, we end up with the sought-after parameters V_{00}^{nn} representing $V_\mu^{(i)}$,

via the relation

$$\langle D_s | V_\mu^{(i)} | B_s \rangle = 2\sqrt{M^{B_s} E^{D_s}} V_{00}^{nn} |_{V=V_\mu^{(i)} \text{ in simulation}} \quad (4.43)$$

We have asserted the ground state of B_s to be it's mass, but not the D_s , as we give D_s spacial momenta in the calculation (to be expanded on in the next section). Then, the full vector currents $\langle D_s | V_\mu^{(i)} | B_s \rangle$ can be build from a linear combination of these according to ??.

4.2.2 The Golden Window

explaination of why t_{cut} is neccesary.

signal/noise degredation as t gets bigger in presence of heavy things or high momenta

One of the main obstacles in our calculation is the *signal degredation* of correlation functions computed on the lattice.

A random variable x has mean and standard deviation

$$\hat{x} = \langle x \rangle \quad (4.44)$$

$$\sigma^2 = \frac{1}{N}(\langle x^2 \rangle - \langle x \rangle^2), \quad (4.45)$$

where N is the size of the sample. So the (square of) the signal/noise ratio is

$$\frac{\hat{x}^2}{\sigma^2} = N \left(\frac{\langle x^2 \rangle}{\langle x \rangle^2} - 1 \right)^{-1}. \quad (4.46)$$

Consider 2 point correlators where $x = \Phi^\dagger(t)\Phi(0)$, where Φ is a meson operator with zero spacial momentum.

$\langle x^2 \rangle$ and $\langle x \rangle$ can be written as

$$\langle x \rangle = \sum_k \frac{1}{2E_n} \langle 0 | \Phi^\dagger(t) | \lambda_n \rangle \langle \lambda_n | \Phi(0) | 0 \rangle e^{-E_n t} \simeq_{t \rightarrow \infty} e^{-E_0 t} \quad (4.47)$$

$$\langle x^2 \rangle = \sum_n \frac{1}{2E_n} \langle 0 | \Phi^{\dagger 2}(t) | \lambda_n \rangle \langle \lambda_n | \Phi^2(0) | 0 \rangle e^{-E_n t} \simeq_{t \rightarrow \infty} e^{-E'_0 t} \quad (4.48)$$

where we have assumed the ratio of matrix elements and energies are $\mathcal{O}(1)$. The two ground state energies E_0 and E'_0 need not be the same, since the lowest states for which $\langle \lambda_n | \Phi(0) | 0 \rangle \neq 0$ and $\langle \lambda_n | \Phi^2(0) | 0 \rangle \neq 0$ may differ.

The operator Φ^2 will contain two quark and two antiquark operators, connected by some matrices in spin space. Φ^2 can create a combination of all possible 2 meson states where the mesons are made of the available quark species, and quantum numbers. For example, If Φ is a pion, Φ^2 is a 2 pion state, and $E'_0 = 2m_\pi$. If Φ is a D_s meson, then $E'_0 = m_{\tilde{\pi}} + m_{\eta_c}$ ($\tilde{\pi}$ is a pseudoscalar $s\bar{s}$ state).

Define $\mu_0 = E'_0/2$. Then

$$\frac{\hat{x}^2}{\sigma^2} \simeq N \left(e^{-2(\mu_0 - m_\Phi)t} - 1 \right)^{-1} \quad (4.49)$$

In the case of pions, $\mu_0 = m_\Phi$, the ratio becomes simply $\sim N$. For mesons heavier than the pion, $\mu_0 < m_\Phi$, so at large times $e^{-2(\mu_0 - m_\Phi)t} \gg 1$, and upon taylor expanding the inverse of this phase we arrive at

$$\frac{\hat{x}}{\sigma} \simeq \sqrt{N} e^{-(m_\varphi - \mu_0)t} \quad (4.50)$$

From this we see there are 3 variables which effect the quality of the signal:

1. The size of the sample N .
2. At large t , the correlators undergo *signal degradation*, i.e., become dominated by noise.
3. The degree of signal degradation is decided by $m_\varphi - \mu_0$. Heavier mesons will tend to experience more signal degradation.

Relevant to our calculation is how giving mesons non-zero spacial momenta \underline{p} can exacerbate this problem. In this case, m_Φ in (4.50) is replaced with $\sqrt{m_\Phi^2 + \underline{p}^2}$. As \underline{p} increases, the signal/noise ratio will degrade more and more and statistics will suffer.

In the $B_s \rightarrow D_s l \nu$ calculation, to deduce form factors over the whole range of q^2 values, we need to simulate the process with the D_s having a range of momenta $0 < |\underline{p}| < 2.32 \text{ GeV}$, as discussed in sec. ???. Correlation functions at the higher end of this range may be too noisy for any meaningful results to be extracted. We are investigating ways of taming this problem, see sec. ??.

4.3 Renormalization of Currents

general principle of matching factors

Once one has computed a matrix element from a lattice calculation, it needs to be translated into a continuum regularization scheme. Suppose we have some bare operator \mathcal{O}_0 , we expect this to be related to the renormalized operator in \overline{MS} at scale μ , $\mathcal{O}^{\overline{MS}}(\mu)$, via

$$\mathcal{O}^{\overline{MS}}(\mu) = Z^{\overline{MS}}(\mu)\mathcal{O}_0. \quad (4.51)$$

Similarly, in a lattice regularization,

$$\mathcal{O}^{\text{lat}}(1/a) = Z^{\text{lat}}(1/a)\mathcal{O}_0. \quad (4.52)$$

Hence we expect a multiplicative factor between the lattice matrix elements, and the continuum \overline{MS} ones:

$$\langle \mathcal{O} \rangle^{\overline{MS}} = \mathcal{Z}(\mu, 1/a) \langle \mathcal{O} \rangle^{\text{lat}} \quad (4.53)$$

where $\mathcal{Z}(\mu, 1/a) = Z^{\overline{MS}}(\mu)/Z^{\text{lat}}(1/a)$. These "matching factors" \mathcal{Z} can be deduced by equating observables calculated in both lattice QCD and continuum (appropriately regularized) QCD, producing equations which can be solved for \mathcal{Z} . The lattice side of the calculation can be done either through lattice perturbation theory ("perturbative matching"), or through a simulation ("non-perturbative matching").

It is a well-known result that conserved (or partially conserved) currents do not receive any renormalization in any scheme, i.e. $Z^{\text{any}} = 1$ ("absolutely normalized").

In principle this is of great help, since the currents we are calculating, namely V_μ , are partially conserved, so we are not required to include any matching factors. However in practice, this is complicated by the fact that the conserved current in the lattice theory is often computationally difficult or impossible to compute. For example, in NRQCD, the partially conserved current corresponding to $SU(N)_V$ is an infinite sum in $1/m_b$ where m_b is the bottom mass. The corresponding current in HISQ is also the sum of a large number of operators. This can be interpreted as a mixing in the renormalization:

$$\langle \mathcal{O}_i \rangle^{\overline{MS}} = \mathcal{Z}_{i,j} \langle \mathcal{O}_j \rangle^{\text{lat}} \quad (4.54)$$

In practice, lattice calculations often use only the dominant operators that contribute to the conserved current. Since these will be "close" to the conserved current, one can expect the matching factor to only be a small deviation from unity,

and the more sub-dominant operators you add, the overall matching factor should tend towards one.

4.3.1 Non-perturbative Renormalization of HISQ Currents

$(m_1 - m_2)S$ absolutely normalised,

V, A normalisations via ward identities

4.3.2 Matching NRQCD currents to \overline{MS}

list currently available matching factors,

mention what isn't available, where we need to truncate the series of currents, the issues this brings up.

CHAPTER 5

b -Physics from Lattice NRQCD

5.1 $B_{(s)} \rightarrow D_{(s)} l \nu$ Form Factors

brief motivation

disclaimer: this was never properly finished! (is it ok to say this?)

5.1.1 Calculation Setup

ensemble details, what correlators were calculated, etc.

5.1.2 Results

as far as I got : plots of form factors

discuss how too many correlators makes the fits very unstable...

5.1.3 The Subleading Current Problem

Talk about the fact that $J_k^{(3,4)}$ are huge, how there isn't much way around this

5.2 Nonperturbative Renormalisation

5.2.1 Relativistic Normalisation of the $b \rightarrow c$ Axial Current

brief description of what we were trying to do: test normalisations, or fix new normalisations

results - plots of $a_0(p)/a_0(0)$ against p^2

why it didn't work

5.2.2 $b \rightarrow c$ Vector Current Matching to Heavy-HISQ

Explain that $B_c \rightarrow \eta_c$ data from both heavy-HISQ and NRQCD were available, ref. Andrew & Brian.

Fix normalisation of V_0 by comparing f_0/f_{B_c} at zero recoil at $q^2 = 0$.

CHAPTER 6

$B_s \rightarrow D_s^* l \nu$ Axial Form Factor at Zero Recoil from Heavy-HISQ

brief motivation, V_{cb} etc.

6.1 Calculation Setup

ensembles, masses, etc. used

basically going to repurpose paper in here

6.2 Results

6.3 Implications for $B \rightarrow D^* l \nu$ and $|V_{cb}|$

$B \rightarrow D^*$, fermilab data plot, how it relates to $|V_{cb}|$ tensions etc.

CHAPTER 7

$B_s \rightarrow D_s l \nu$ Form Factor at All Physical q^2 from Heavy-HISQ

brief motivation, V_{cb} etc.

7.1 Calculation Setup

basically repurpose paper again

7.2 Results

7.3 HQET low energy constants

won't mention this in the paper, but i did some work fitting h_+ to the HQET expression, similar to in the $Bs - Ds^*$ case

List of Figures

2.1	The flavour-changing charged current vertex.	8
2.2	A sketch of the unitarity triangle.	10
2.3	Exclusion regions for the vertices of the CKM triangle from various measurements, courtesy of the most recent PDG update [1].	11
2.4	Leptonic decay of meson M at tree level in the electroweak coupling.	12
2.5	Semileptonic decay, $M \rightarrow M' l \bar{\nu}$, at tree level in electroweak coupling.	13
2.6	Different determinations of $ V_{cb} $. Points labelled $w = 1$ are determinations from extrapolating measurements of decay rates to the zero recoil point, and combined with a lattice determination of the form factor at zero recoil. Points labelled $w \geq 1$ are results from using a combination of both branching fractions and lattice form factors through some range of w . The first name mentioned in the labels give the source of the lattice form factors, and the second gives the source of the experimental data (e.g. the HPQCD+BaBar point used form factors from the HPQCD collaboration and data from the BaBar experiment. The highest point is from [5], the second and third highest from [6], fourth from [7], fifth from [8]. The bottom point is from the PDG [1], using data from the ALPEPH [9], Belle [10], BaBar [11, 12], and CLEO [13] experiments.	17
2.7	$R(D^{(*)})$ determinations from SM and measurement [26].	19
2.8	The relationship between scale Q and the strong coupling constant α_s , from the PDG [1].	23
3.1	Depiction of colour spaces (fibres) at two points in spactime (base space) with the value of the quark field q represented at each point as a colour vector, and the connection $W(x, y)$ needed to compare the two colour vectors. A gauge transform changes the two vectors in different ways, for the comparison to be gauge independent, the connection must also transform appropriately.	36
3.2	Depiction of a gauge invariant quark bilinear, connected by a Wilson line made of gauge links.	36
3.3	Elementary Plaquette.	37

3.4	Terms additional to the elementary plaquette in the improved pure QCD action.	39
3.5	Illustration of isolating a single taste via a doubling symmetry transformation \mathcal{B}_ζ then a block-scaling.	43
3.6	Taste mixing at tree level.	45
3.7	Different scales relevant to non-perturbative physics.	47
3.8	An extrapolation to $m_h = m_b$ of the η_h decay constant (where η_h is a pseudoscalar $\bar{h}h$ meson [66]. The colourful points are measurements of f_{η_h} on the lattice, the colour denotes lattice spacing and the x axis, M_{η_h} , is a proxy for the h -quark mass.	48

List of Tables

Bibliography

- [1] M. et. al. Tanabashi. Review of particle physics. *Phys. Rev. D*, 98:030001, Aug 2018.
- [2] Bugra Borasoy. Introduction to Chiral Perturbation Theory. *Springer Proc. Phys.*, 118:1–26, 2008.
- [3] Ikaros I. Y. Bigi, Mikhail A. Shifman, N. Uraltsev, and Arkady I. Vainshtein. High power n of m_b in beauty widths and $n = 5 \rightarrow \infty$ limit. *Phys. Rev.*, D56:4017–4030, 1997. [,205(1996)].
- [4] Andre H. Hoang, Zoltan Ligeti, and Aneesh V. Manohar. B decays in the upsilon expansion. *Phys. Rev.*, D59:074017, 1999.
- [5] Heechang Na, Chris M. Bouchard, G. Peter Lepage, Chris Monahan, and Junko Shigemitsu. $B \rightarrow Dl\nu$ form factors at nonzero recoil and extraction of $|V_{cb}|$. *Phys. Rev.*, D92(5):054510, 2015. [Erratum: *Phys. Rev.*D93,no.11,119906(2016)].
- [6] Jon A. Bailey et al. $B \rightarrow Dl\nu$ form factors at nonzero recoil and $|V_{cb}|$ from 2+1-flavor lattice QCD. *Phys. Rev.*, D92(3):034506, 2015.
- [7] Jon A. Bailey et al. Update of $|V_{cb}|$ from the $\bar{B} \rightarrow D^*\ell\bar{\nu}$ form factor at zero recoil with three-flavor lattice QCD. *Phys. Rev.*, D89(11):114504, 2014.
- [8] Benjamin Grinstein and Andrew Kobach. Model-Independent Extraction of $|V_{cb}|$ from $\bar{B} \rightarrow D^*\ell\bar{\nu}$. *Phys. Lett.*, B771:359–364, 2017.
- [9] D Buskulic et. al. A measurement of $|v_{cb}|$ from $b^0 \rightarrow d^*l^-\nu_l$. *Physics Letters B*, 359(1):236 – 248, 1995.
- [10] Kazuo Abe et al. Measurement of $B(\text{anti-}B^0 \rightarrow D^+ l^- \text{anti-}\nu_l)$ and determination of $|V(cb)|$. *Phys. Lett.*, B526:258–268, 2002.
- [11] Bernard Aubert et al. Measurements of the Semileptonic Decays $\text{anti-}B \rightarrow D l \text{ anti-}\nu_l$ and $\text{anti-}B \rightarrow D^* l \text{ anti-}\nu_l$ Using a Global Fit to $D \times l \text{ anti-}\nu_l$ Final States. *Phys. Rev.*, D79:012002, 2009.

- [12] Bernard Aubert et al. Measurement of $|V(cb)|$ and the Form-Factor Slope in $B \rightarrow D l^- \bar{\nu}_l$ Decays in Events Tagged by a Fully Reconstructed B Meson. *Phys. Rev. Lett.*, 104:011802, 2010.
- [13] John E. Bartelt et al. Measurement of the $B \rightarrow D$ lepton neutrino branching fractions and form-factor. *Phys. Rev. Lett.*, 82:3746, 1999.
- [14] Dante Bigi, Paolo Gambino, and Stefan Schacht. A fresh look at the determination of $|V_{cb}|$ from $B \rightarrow D^* \ell \nu$. *Phys. Lett.*, B769:441–445, 2017.
- [15] Jon A. Bailey, Sunkyu Lee, Weonjong Lee, Jaehoon Leem, and Sungwoo Park. Updated evaluation of ϵ_K in the standard model with lattice QCD inputs. *Phys. Rev.*, D98(9):094505, 2018.
- [16] J. P. Lees et al. Evidence for an excess of $\bar{B} \rightarrow D^{(*)} \tau^- \bar{\nu}_\tau$ decays. *Phys. Rev. Lett.*, 109:101802, 2012.
- [17] J. P. Lees et al. Measurement of an Excess of $\bar{B} \rightarrow D^{(*)} \tau^- \bar{\nu}_\tau$ Decays and Implications for Charged Higgs Bosons. *Phys. Rev.*, D88(7):072012, 2013.
- [18] M. Huschle et al. Measurement of the branching ratio of $\bar{B} \rightarrow D^{(*)} \tau^- \bar{\nu}_\tau$ relative to $\bar{B} \rightarrow D^{(*)} \ell^- \bar{\nu}_\ell$ decays with hadronic tagging at Belle. *Phys. Rev.*, D92(7):072014, 2015.
- [19] Y. Sato et al. Measurement of the branching ratio of $\bar{B}^0 \rightarrow D^{*+} \tau^- \bar{\nu}_\tau$ relative to $\bar{B}^0 \rightarrow D^{*+} \ell^- \bar{\nu}_\ell$ decays with a semileptonic tagging method. *Phys. Rev.*, D94(7):072007, 2016.
- [20] S. Hirose et al. Measurement of the τ lepton polarization and $R(D^*)$ in the decay $\bar{B} \rightarrow D^* \tau^- \bar{\nu}_\tau$. *Phys. Rev. Lett.*, 118(21):211801, 2017.
- [21] S. Hirose et al. Measurement of the τ lepton polarization and $R(D^*)$ in the decay $\bar{B} \rightarrow D^* \tau^- \bar{\nu}_\tau$ with one-prong hadronic τ decays at Belle. *Phys. Rev.*, D97(1):012004, 2018.
- [22] Roel Aaij et al. Measurement of the ratio of branching fractions $\mathcal{B}(\bar{B}^0 \rightarrow D^{*+} \tau^- \bar{\nu}_\tau) / \mathcal{B}(\bar{B}^0 \rightarrow D^{*+} \mu^- \bar{\nu}_\mu)$. *Phys. Rev. Lett.*, 115(11):111803, 2015. [Erratum: Phys. Rev. Lett. 115, no. 15, 159901 (2015)].
- [23] R. Aaij et al. Measurement of the ratio of the $B^0 \rightarrow D^{*-} \tau^+ \nu_\tau$ and $B^0 \rightarrow D^{*-} \mu^+ \nu_\mu$ branching fractions using three-prong τ -lepton decays. *Phys. Rev. Lett.*, 120(17):171802, 2018.

- [24] R. Aaij et al. Test of Lepton Flavor Universality by the measurement of the $B^0 \rightarrow D^{*-} \tau^+ \nu_\tau$ branching fraction using three-prong τ decays. *Phys. Rev.*, D97(7):072013, 2018.
- [25] Svjetlana Fajfer, Jernej F. Kamenik, and Ivan Nisandzic. On the $B \rightarrow D^* \tau \bar{\nu}_\tau$ Sensitivity to New Physics. *Phys. Rev.*, D85:094025, 2012.
- [26] Y. Amhis et al. Averages of b -hadron, c -hadron, and τ -lepton properties as of summer 2016. *Eur. Phys. J.*, C77:895, 2017. updated results and plots available at <https://hflav.web.cern.ch><https://hflav.web.cern.ch>.
- [27] Wolfgang Altmannshofer, Peter Stangl, and David M. Straub. Interpreting Hints for Lepton Flavor Universality Violation. *Phys. Rev.*, D96(5):055008, 2017.
- [28] Roel Aaij et al. Test of lepton universality using $B^+ \rightarrow K^+ \ell^+ \ell^-$ decays. *Phys. Rev. Lett.*, 113:151601, 2014.
- [29] Marzia Bordone, Gino Isidori, and Andrea Patti. On the Standard Model predictions for R_K and R_{K^*} . *Eur. Phys. J.*, C76(8):440, 2016.
- [30] Sébastien Descotes-Genon, Lars Hofer, Joaquim Matias, and Javier Virto. Global analysis of $b \rightarrow s \ell \ell$ anomalies. *JHEP*, 06:092, 2016.
- [31] Bernat Capdevila, Sébastien Descotes-Genon, Joaquim Matias, and Javier Virto. Assessing lepton-flavour non-universality from $B \rightarrow K^* \ell \ell$ angular analyses. *JHEP*, 10:075, 2016.
- [32] Bernat Capdevila, Sébastien Descotes-Genon, Lars Hofer, and Joaquim Matias. Hadronic uncertainties in $B \rightarrow K^* \mu^+ \mu^-$: a state-of-the-art analysis. *JHEP*, 04:016, 2017.
- [33] Nicola Serra, Rafael Silva Coutinho, and Danny van Dyk. Measuring the breaking of lepton flavor universality in $B \rightarrow K^* \ell^+ \ell^-$. *Phys. Rev.*, D95(3):035029, 2017.
- [34] Aoife Bharucha, David M. Straub, and Roman Zwicky. $B \rightarrow V \ell^+ \ell^-$ in the Standard Model from light-cone sum rules. *JHEP*, 08:098, 2016.
- [35] Wolfgang Altmannshofer, Christoph Niehoff, Peter Stangl, and David M. Straub. Status of the $B \rightarrow K^* \mu^+ \mu^-$ anomaly after Moriond 2017. *Eur. Phys. J.*, C77(6):377, 2017.

- [36] Sebastian Jäger and Jorge Martin Camalich. Reassessing the discovery potential of the $B \rightarrow K^* \ell^+ \ell^-$ decays in the large-recoil region: SM challenges and BSM opportunities. *Phys. Rev.*, D93(1):014028, 2016.
- [37] R. Aaij et al. Test of lepton universality with $B^0 \rightarrow K^{*0} \ell^+ \ell^-$ decays. *JHEP*, 08:055, 2017.
- [38] Kazuo Abe et al. An Upper bound on the decay tau —> mu gamma from Belle. *Phys. Rev. Lett.*, 92:171802, 2004.
- [39] A. M. Baldini et al. Search for the lepton flavour violating decay $\mu^+ \rightarrow e^+ \gamma$ with the full dataset of the MEG experiment. *Eur. Phys. J.*, C76(8):434, 2016.
- [40] Marat Freytsis, Zoltan Ligeti, and Joshua T. Ruderman. Flavor models for $\bar{B} \rightarrow D^{(*)} \tau \bar{\nu}$. *Phys. Rev.*, D92(5):054018, 2015.
- [41] Martin Bauer and Matthias Neubert. Minimal Leptoquark Explanation for the $R_{D^{(*)}}$, R_K , and $(g - 2)_g$ Anomalies. *Phys. Rev. Lett.*, 116(14):141802, 2016.
- [42] Andreas Crivellin, Giancarlo D'Ambrosio, and Julian Heeck. Explaining $h \rightarrow \mu^\pm \tau^\mp$, $B \rightarrow K^* \mu^+ \mu^-$ and $B \rightarrow K \mu^+ \mu^- / B \rightarrow K e^+ e^-$ in a two-Higgs-doublet model with gauged $L_\mu - L_\tau$. *Phys. Rev. Lett.*, 114:151801, 2015.
- [43] Matthew D. Schwartz. *Quantum Field Theory and the Standard Model*. Cambridge University Press, 2014.
- [44] I.S. Altarev, Yu.V. Borisov, N.V. Borovikova, S.N. Ivanov, E.A. Kolomensky, M.S. Lasakov, V.M. Lobashev, V.A. Nazarenko, A.N. Pirozhkov, A.P. Serebrov, Yu.V. Sobolev, E.V. Shulgina, and A.I. Yegorov. New measurement of the electric dipole moment of the neutron. *Physics Letters B*, 276(1):242 – 246, 1992.
- [45] David J. Gross and Frank Wilczek. Ultraviolet behavior of non-abelian gauge theories. *Phys. Rev. Lett.*, 30:1343–1346, Jun 1973.
- [46] Stefan Scherer. Introduction to chiral perturbation theory. *Adv. Nucl. Phys.*, 27:277, 2003. [,277(2002)].
- [47] S. Fubini and G. Furlan. Renormalization effects for partially conserved currents. *Physics Physique Fizika*, 1(4):229–247, 1965.

- [48] Richard F. Lebed and Mahiko Suzuki. Current algebra and the Ademollo-Gatto theorem in spin flavor symmetry of heavy quarks. *Phys. Rev.*, D44:829–836, 1991.
- [49] Leslie L. Foldy and Siegfried A. Wouthuysen. On the dirac theory of spin 1/2 particles and its non-relativistic limit. *Phys. Rev.*, 78:29–36, Apr 1950.
- [50] G. Peter Lepage, Lorenzo Magnea, Charles Nakhleh, Ulrika Magnea, and Kent Hornbostel. Improved nonrelativistic QCD for heavy quark physics. *Phys. Rev.*, D46:4052–4067, 1992.
- [51] Philippe de Forcrand. Simulating QCD at finite density. *PoS*, LAT2009:010, 2009.
- [52] M. Lüscher and P. Weisz. On-shell improved lattice gauge theories. *Comm. Math. Phys.*, 97(1-2):59–77, 1985.
- [53] P. Weisz. Continuum limit improved lattice action for pure yang-mills theory (i). *Nuclear Physics B*, 212(1):1 – 17, 1983.
- [54] P. Weisz and R. Wohlert. Continuum limit improved lattice action for pure yang-mills theory (ii). *Nuclear Physics B*, 236(2):397 – 422, 1984.
- [55] A. Hart, G. M. von Hippel, and R. R. Horgan. Radiative corrections to the lattice gluon action for HISQ improved staggered quarks and the effect of such corrections on the static potential. *Phys. Rev.*, D79:074008, 2009.
- [56] Kenneth G. Wilson. Confinement of Quarks. *Phys. Rev.*, D10:2445–2459, 1974. [,319(1974)].
- [57] John B. Kogut and Leonard Susskind. Hamiltonian Formulation of Wilson’s Lattice Gauge Theories. *Phys. Rev.*, D11:395–408, 1975.
- [58] E. Follana, Q. Mason, C. Davies, K. Hornbostel, G. P. Lepage, J. Shigemitsu, H. Trottier, and K. Wong. Highly improved staggered quarks on the lattice, with applications to charm physics. *Phys. Rev.*, D75:054502, 2007.
- [59] C. T. H. Davies et al. Precision charm physics, $m(c)$ and $\alpha(s)$ from lattice QCD. *PoS*, LATTICE2008:118, 2008.
- [60] C. T. H. Davies. Precision charmonium and D physics from lattice QCD and determination of the charm quark mass. In *Proceedings, 34th International*

Conference on High Energy Physics (ICHEP 2008): Philadelphia, Pennsylvania, July 30-August 5, 2008.

- [61] Jonna Koponen, Christine T. H. Davies, Gordon Donald, Eduardo Follana, G. Peter Lepage, Heechang Na, and Junko Shigemitsu. The D to K and D to pi semileptonic decay form factors from Lattice QCD. *PoS*, LATTICE2011:286, 2011.
- [62] Heechang Na, Christine T. H. Davies, Eduardo Follana, Jonna Koponen, G. Peter Lepage, and Junko Shigemitsu. $D \rightarrow \pi, l\nu$ Semileptonic Decays, $|V_{cd}|$ and 2nd Row Unitarity from Lattice QCD. *Phys. Rev.*, D84:114505, 2011.
- [63] Heechang Na, Chris Monahan, Christine Davies, Eduardo Follana, Ron Horgan, Peter Lepage, and Junko Shigemitsu. Precise Determinations of the Decay Constants of B and D mesons. *PoS*, LATTICE2012:102, 2012.
- [64] Heechang Na, Christine T. H. Davies, Eduardo Follana, G. Peter Lepage, and Junko Shigemitsu. $|V_{cd}|$ from D Meson Leptonic Decays. *Phys. Rev.*, D86:054510, 2012.
- [65] Jonna Koponen. Lattice results for D/D_s leptonic and semileptonic decays. In *Proceedings, 6th International Workshop on Charm Physics (Charm 2013): Manchester, UK, August 31-September 4, 2013*, 2013.
- [66] C. McNeile, C. T. H. Davies, E. Follana, K. Hornbostel, and G. P. Lepage. Heavy meson masses and decay constants from relativistic heavy quarks in full lattice QCD. *Phys. Rev.*, D86:074503, 2012.
- [67] Andrew Lytle, Brian Colquhoun, Christine Davies, Jonna Koponen, and Craig McNeile. Semileptonic B_c decays from full lattice QCD. *PoS*, BEAUTY2016:069, 2016.
- [68] A. Gray, I. Allison, C. T. H. Davies, Emel Dalgic, G. P. Lepage, J. Shigemitsu, and M. Wingate. The Upsilon spectrum and m(b) from full lattice QCD. *Phys. Rev.*, D72:094507, 2005.
- [69] Christine T. H. Davies, Judd Harrison, Ciaran Hughes, Ronald R. Horgan, Georg M. von Hippel, and Matthew Wingate. Improving the Kinetic Couplings in Lattice Non-Relativistic QCD. 2018.

- [70] R. J. Dowdall et al. The Upsilon spectrum and the determination of the lattice spacing from lattice QCD including charm quarks in the sea. *Phys. Rev.*, D85:054509, 2012.
- [71] Michael E. Peskin and Daniel V. Schroeder. *An Introduction to quantum field theory*. 1995.
- [72] Thomas DeGrand and Carleton E. Detar. *Lattice methods for quantum chromodynamics*. 2006.
- [73] A. Bazavov et al. Lattice QCD ensembles with four flavors of highly improved staggered quarks. *Phys. Rev.*, D87(5):054505, 2013.
- [74] G.P.Lepage. Corrfitter: <https://github.com/gplepage/corrfitter>, 2012.
- [75] B. Colquhoun, C. T. H. Davies, R. J. Dowdall, J. Kettle, J. Koponen, G. P. Lepage, and A. T. Lytle. B-meson decay constants: a more complete picture from full lattice QCD. *Phys. Rev.*, D91(11):114509, 2015.
- [76] Christopher J Monahan, Heechang Na, Chris M Bouchard, G Peter Lepage, and Junko Shigemitsu. $B_s \rightarrow D_s \ell \nu$ Form Factors and the Fragmentation Fraction Ratio f_s/f_d . 2017.